Research Square

Preprints are preliminary reports that have not undergone peer review.
They should not be considered conclusive, used to inform clinical practice,
or referenced by the media as validated information.

Mesoporous nano-silica, nano-iron, and Ascophyllum nodosum extract enhance nutrient uptake and salt tolerance in maize

Wasimah B. Al-Shammari
University of Hail
Haya Altamimi
University of Hail
Dalal Alenizi
University of Hail
Kholoud Alshammery
University of Hail
Jawaher Alrashdi
University of Hail
Hanan Khalaf Anazi
University of Tabuk
Habibah A Almalawi
University of Tabuk
Mona H. Soliman
hmona@sci.cu.edu.eg
Cairo University

Research Article

Keywords: Salinity stress, maize, mesoporous nano-silica, nano-iron, Ascophyllum nodosum extract, antioxidant defense, photosynthesis, ion homeostasis, molecular adaptation

Posted Date: November 19th, 2026

DOI: https://doi.org/10.21203/rs.3.rs-11398619/v1

License: This work is licensed under a Creative Commons Attribution 4.0 International License.
Read Full License

Additional Declarations: No competing interests reported.

Mesoporous nano-silica, nano-iron, and *Ascophyllum nodosum* extract enhance nutrient uptake and salt tolerance in maize

Wasimah B. Al-Shammari[1], Haya Altamimi[1], Dalal Alenizi[1], Kholoud Alshammery[1], Jawaher Alrashdi[1], Hanan Khalaf Anazi[2], Habibah A Almalawi[2], Mona H. Soliman [3,4*]

[1]Department of Biology, College of Science, University of Hail, P.O. Box 2440, Hail, 55476, Saudi Arabia; w.alshamary@uoh.edu.sa; h.altamyme@uoh.edu.sa; d.aloneze@uoh.edu.sa; dr.khloud@uoh.edu.sa; g.alrashidi@uoh.edu.sa

[2]Department of Biology, Faculty of Sciences, University of Tabuk, Tabuk, 71491, Saudi Arabia; hkalenazi@ut.edu.sa; halmalawi@ut.edu.sa

[3]Botany and Microbiology Department, Faculty of Science, Cairo University, Giza 12613, Egypt; hmona@sci.cu.edu.eg

[4]Department of Biology, College of Science in Yanbu, Taibah University, Yanbu Governorate, Saudi Arabia; mhhussein@taibahu.edu.sa

[*]Corresponding author: Dr. Mona H. Soliman: hmona@sci.cu.edu.eg

Abstract

Salinity restricts maize (*Zea mays* L.) productivity by disrupting photosynthesis, nutrient acquisition, ionic balance, and redox homeostasis. This study investigated whether mesoporous nano-silica (MNS), nano-iron (Nano-Fe), and *Ascophyllum nodosum* extract (ANE), applied alone or combined, could enhance maize tolerance to salinity. A factorial experiment was conducted in a completely randomized design under 0, 75, and 150 mM NaCl. Morphological, physiological, biochemical, gas-exchange, antioxidant, and stress-responsive molecular traits were evaluated. Salinity reduced plant height, fresh biomass, total chlorophyll, and net photosynthetic rate by 43.5%, 54.2%, 48.3%, and 60.7%, respectively, while increasing Na^+ accumulation, osmotic stress, and oxidative damage. The combined MNS + Nano-Fe + ANE treatment provided the greatest protection, increasing plant height, fresh and dry biomass, and net photosynthetic rate by 47.8%, 72.0%, 101.9%, and 145.5%, respectively, relative to untreated plants at 150 mM NaCl. It improved chlorophyll retention, osmolyte and soluble-protein accumulation, antioxidant capacity, nutrient uptake, and ionic homeostasis while reducing malondialdehyde, hydrogen peroxide, and Na^+ toxicity. Salinity induced *ZmDREB2A*, *ZmHSP70*, *ZmP5CS*, *ZmCAT1*, and *ZmNHX1*, reflecting activation of stress signaling, osmotic adjustment, antioxidant defense, and ion transport.

The combined treatment strengthened adaptive transcription under moderate salinity but moderated gene induction under severe stress, indicating improved homeostasis. Correlation analysis linked photosynthesis and nutrient accumulation positively with antioxidant and molecular responses and negatively with oxidative-stress markers. These findings demonstrate that integrating MNS, Nano-Fe, and ANE enhances maize salinity tolerance through photosynthetic protection, ion regulation, osmotic adjustment, reactive-oxygen-species detoxification, and molecular adaptation, offering a promising strategy for crop production in salt-affected soils.

Keywords: Salinity stress; maize; mesoporous nano-silica; nano-iron; *Ascophyllum nodosum* extract; antioxidant defense; photosynthesis; ion homeostasis; molecular adaptation

Introduction

Salinity stress is a major environmental factor limiting maize (*Zea mays* L.) productivity, particularly in arid and semi-arid regions, by inducing osmotic stress, ionic toxicity, nutrient imbalance, and metabolic dysfunction. Excessive accumulation of Na^+ and Cl^- reduces water uptake, disrupts membrane stability, inhibits photosynthesis through chlorophyll degradation and stomatal closure, and ultimately suppresses plant growth and yield (Islam et al. 2024). Salinity also enhances the overproduction of reactive oxygen species (ROS), including superoxide radicals, hydrogen peroxide, and hydroxyl radicals, which cause oxidative damage to lipids, proteins, nucleic acids, and cellular membranes, often reflected by increased malondialdehyde (MDA) accumulation (Ahmad et al. 2019; Alshammari et al. 2024). Although plants activate antioxidant defense systems such as superoxide dismutase (SOD), catalase (CAT), ascorbate peroxidase (APX), and polyphenol oxidase (PPO), severe salinity can overwhelm these protective mechanisms, leading to oxidative stress and cellular injury (Rao et al. 2025; Al-Shammari et al. 2024). In addition, salinity disrupts nutrient uptake and ion homeostasis by interfering with the absorption and transport of essential nutrients such as potassium, calcium, magnesium, and micronutrients (Awais et al. 2023; Al-Shammari et al. 2025), thereby impairing osmotic regulation, enzyme activation, chlorophyll biosynthesis, and overall physiological performance. Collectively, these physiological, biochemical, and molecular disturbances substantially reduce maize growth, productivity, and stress tolerance under saline conditions.

In recent years, nanotechnology has emerged as a promising and innovative approach for improving plant performance under abiotic stress conditions (Weisany et al. 2024). Nanoparticles possess unique physicochemical properties including small particle size, large surface area, high reactivity, and enhanced penetration capacity, enabling more efficient interaction with plant tissues compared with conventional fertilizers and amendments (Aqaei et al. 2020; Weisany and Khosropour 2023). Among different nanomaterials, silicon- and iron-based nanoparticles have received considerable attention because of their beneficial roles in stress tolerance and nutrient metabolism (Ghouri et al. 2024; Weisany et al. 2023).

In addition to nanotechnology-based approaches, biostimulants have gained increasing attention as sustainable tools for improving crop tolerance to environmental stress (Johnson et al. 2024; Darakeh et al. 2022). Seaweed extracts, particularly those derived from *Ascophyllum nodosum*, are among the most widely used commercial biostimulants in agriculture (Shukla et al. 2019). *A. nodosum* extract (ANE) contains a broad range of bioactive compounds including phytohormones, amino acids, polysaccharides, betaines, vitamins, phenolic compounds, antioxidants, and mineral nutrients (Kumari et al. 2023). These compounds stimulate plant growth, improve nutrient uptake, enhance antioxidant defense systems, and regulate stress-responsive signaling pathways. ANE has been reported to improve photosynthesis, root development, osmotic adjustment, membrane stability, and enzyme activity under salinity (Dell'Aversana et al. 2021), drought (Goñi et al. 2018), and temperature stress (Repke et al. 2022) conditions. Furthermore, seaweed-derived polysaccharides and osmoprotectants contribute to improved cellular hydration and ROS scavenging under saline environments (Dang et al. 2026).

Although previous studies have separately examined the roles of silicon nanoparticles, iron nanoparticles, and seaweed extracts in enhancing plant tolerance to salinity stress, their combined and interactive effects in maize remain insufficiently explored. Most research has focused on the individual application of nanoparticles or biostimulants, leaving the potential synergistic mechanisms largely unclear. The combined use of MNS, Nano-Fe, and ANE may offer complementary benefits by simultaneously enhancing membrane stability, nutrient uptake, osmotic adjustment, antioxidant defense, photosynthetic performance, and stress-responsive signaling. Silicon can improve ion homeostasis and structural protection, while nano-iron supports chlorophyll synthesis, electron transport, and enzymatic functions. In parallel, ANE provides

phytohormones, amino acids, polysaccharides, and antioxidant compounds that activate cellular defense pathways and metabolic adaptation. Therefore, integrating these nano-enabled biostimulants represents a promising and sustainable strategy for improving maize resilience and productivity under saline conditions.

The novelty of this study lies in evaluating the integrated application of MNS, Nano-Fe, and ANE as a comprehensive nano-biostimulant system to mitigate salinity stress in maize. Few studies have simultaneously investigated their effects on plant growth, oxidative stress regulation, nutrient balance, photosynthetic efficiency, antioxidant metabolism, gas exchange, and stress-responsive gene expression under varying salinity levels. By combining physiological, biochemical, nutritional, antioxidant, and molecular analyses, this research provides mechanistic insights into how nano-silica-mediated structural protection, nano-iron-induced metabolic activation, and ANE-derived bioactive signaling collectively enhance salinity tolerance. Given the rapid expansion of salt-affected soils worldwide and the limitations of conventional fertilizers under saline environments, this study also highlights the potential of environmentally friendly nano-biostimulant technologies to improve nutrient-use efficiency, reduce environmental impacts, and support sustainable maize production in arid and marginal lands.

Material and methods

Experimental Design and Plant Growth Conditions

The experiment was conducted with maize (*Zea mays* L.) under controlled greenhouse conditions using a factorial arrangement in a completely randomized design. The experimental factors were salinity stress, nanoparticle application, and biostimulant treatment. Uniform, healthy seeds were obtained from the Ministry of Environment, Water and Agriculture, Saudi Arabia. Before sowing, the seeds were surface-sterilized by immersion in 1% (v/v) sodium hypochlorite for 3 min and subsequently rinsed five times with distilled water to remove any residual disinfectant. The sterilized seeds were then sown in plastic pots containing the designated growth substrate and maintained under controlled greenhouse conditions throughout the experimental period.

Salinity stress was imposed at three levels consisting of 0 mM NaCl as the non-saline control, 75 mM NaCl representing moderate salinity stress, and 150 mM NaCl representing severe salinity

stress. The nanoparticle factor included four treatment levels comprising no nanoparticle application, MNS, Nano-Fe, and the combined application of MNS + Nano-Fe. In addition, the biostimulant factor consisted of two levels, including untreated plants and foliar application of ANE. Based on the combination of the three experimental factors, the study included a total of 24 treatment combinations (3 salinity levels × 4 nanoparticle treatments × 2 biostimulant treatments). Each treatment was replicated four times, resulting in a total of 96 experimental units.

Mesoporous nano-silica was applied at a concentration of 100 mg L^{-1}, whereas nano-iron was applied at 50 mg L^{-1}. The *A. nodosum* extract was prepared at a concentration of 2 g L^{-1} and applied as a foliar spray. Prior to application, nanoparticle suspensions were ultrasonicated for 20–30 min to ensure homogeneous dispersion and minimize nanoparticle aggregation. Foliar applications were performed using a hand sprayer until complete runoff at the 3–4 leaf stage, and the treatments were repeated at 10-day intervals during the experimental period to maintain continuous nanoparticle and biostimulant availability.

Salinity treatments were initiated one week after seedling establishment by irrigating the plants with NaCl solutions corresponding to the designated salinity levels. To avoid osmotic shock and ensure gradual acclimation of maize seedlings to saline conditions, salinity levels were increased progressively in increments of 25 mM NaCl per day until the target concentrations of 75 and 150 mM NaCl were achieved.

Plants were grown in a greenhouse under controlled environmental conditions with day/night temperatures maintained at 25 ± 2°C and 18 ± 2°C, respectively, a relative humidity of 60–70%, and a 14-h light/10-h dark photoperiod. Pots were filled with a homogenized growth substrate consisting of loam soil, sand, and peat moss mixed at a ratio of 2:1:1 (v/v/v). Selected physicochemical properties of the growth medium are presented in Table 1. Throughout the experimental period, plants were irrigated regularly to maintain the soil moisture content at approximately 70–80% of field capacity, thereby minimizing moisture fluctuations and ensuring optimal growth conditions.

At the end of the experimental period, a comprehensive evaluation of plant responses was conducted. Morphological parameters including plant height, fresh biomass, dry biomass, and leaf development were measured. Physiological and photosynthetic traits including chlorophyll pigments, gas exchange characteristics, and water relations were also determined. In addition,

biochemical analyses were performed to quantify oxidative stress indicators, osmolyte accumulation, antioxidant enzyme activities, and soluble proteins. Nutrient uptake, ion homeostasis, and mineral element accumulation were assessed to evaluate salinity-induced ionic imbalance and nutrient status. Furthermore, molecular analyses involving the expression of stress-responsive genes associated with antioxidant defense, osmotic adjustment, and ion transport regulation were conducted to elucidate the physiological and molecular mechanisms underlying the mitigation of salinity stress in maize plants following nanoparticle and biostimulant application.

Ascophyllum nodosum Extract

A. nodosum (L.) Le Jolis is a perennial brown macroalga belonging to the family Fucaceae and is naturally distributed primarily along the cold temperate coasts of the North Atlantic Ocean. It is widely used in agricultural biostimulant production because it contains numerous bioactive constituents, including alginates, fucoidans, laminarins, betaines, mannitol, polyphenols, minerals, and phytohormone-like compounds.

Collection, Preparation, Extraction, and Characterization

Fresh thalli provisionally identified as *A. nodosum* were collected in June 2023 from the Red Sea coast near Yanbu Governorate, Saudi Arabia (24°02′16.57″ N, 38°14′11.65″ E). The samples were placed in clean, sealed containers and transported to the laboratory in insulated ice boxes to minimize biochemical deterioration. Taxonomic identification was performed using morphological characteristics and established identification keys (Ghosh and Ghosh 2023). Because the occurrence of *A. nodosum* in the Red Sea is biogeographically unusual, the identification should be supported by a deposited voucher specimen and, where possible, DNA barcoding.

Upon arrival, the algal biomass was washed repeatedly with distilled water to remove adhering sand, salts, epiphytes, and other extraneous materials. The cleaned biomass was shade-dried at room temperature until a constant weight was obtained, thereby minimizing the degradation of thermolabile compounds. The dried material was ground using an electric mill and passed through an 80-mesh sieve to obtain a homogeneous powder. Selected physicochemical characteristics,

including proximate composition and mineral content, were subsequently determined and are presented in Table 2.

For aqueous extraction, 20 g of dried algal powder was suspended in 1 L of distilled water to obtain a concentration of 2% (w/v). The suspension was incubated overnight in a shaking water bath at 60 °C to facilitate the extraction of water-soluble bioactive constituents. After extraction, the mixture was centrifuged at the experimentally verified relative centrifugal force for 20 min. The resulting supernatant was collected, filtered through Whatman No. 1 filter paper, transferred into sterile amber containers, and stored at 4 °C until its use as a foliar biostimulant. The exact centrifugation force, extraction duration, shaking speed, extraction yield, and storage period should be reported to ensure experimental reproducibility.

Proximate composition and mineral analysis

The proximate composition of the dried *Ascophyllum nodosum* biomass was determined using standard analytical procedures described by AOAC International (2019), with modifications appropriate for seaweed matrices (Mæhre et al. 2014). Before analysis, the dried biomass was ground, passed through an 80-mesh sieve, and thoroughly homogenized. All analyses were performed in triplicate, and the results were expressed as mean ± standard deviation.

Moisture content was determined by drying approximately 2 g of the homogenized sample in a forced-air oven at 105 °C until a constant mass was obtained. Moisture content was calculated as follows:

Moisture (%) = [(initial sample mass − oven-dried sample mass) / initial sample mass] × 100

Ash content was measured by incinerating approximately 2 g of the dried sample in a muffle furnace at 550 °C for 5–6 h or until a constant light-grey residue was obtained. The crucibles were cooled in a desiccator before weighing. Ash content was calculated as follows:

Ash (%) = (mass of ash / initial sample mass) × 100

Crude lipid content was determined using Soxhlet extraction. Approximately 2–5 g of the dried sample was extracted with petroleum ether, with a boiling range of 40–60 °C, for 6 h. The solvent was subsequently removed, and the extracted lipid fraction was dried to a constant mass and weighed. Crude lipid content was calculated as follows:

Crude lipid (%) = (mass of extracted lipid / initial sample mass) × 100

Total nitrogen was determined using the Kjeldahl digestion, distillation, and titration method. The sample was digested with concentrated sulfuric acid in the presence of a suitable catalyst until a clear digest was obtained. Following alkalization, the released ammonia was distilled into boric acid and quantified by titration with standardized hydrochloric acid. Crude protein was calculated using a nitrogen-to-protein conversion factor of 6.25.

The use of the term "crude protein" is important because the Kjeldahl procedure measures total nitrogen rather than protein directly. In seaweeds, the conventional factor of 6.25 may overestimate true protein content because the biomass can contain substantial amounts of non-protein nitrogen. Therefore, the conversion factor used should be stated explicitly (Biancarosa et al. 2018).

Crude fibre was determined by sequential acid and alkaline digestion. A defatted sample was first boiled in 1.25% sulfuric acid and then in 1.25% sodium hydroxide. After each digestion, the residue was filtered and washed with hot distilled water. The final residue was dried at 105 °C, weighed, incinerated at 550 °C, cooled in a desiccator, and weighed again. Crude fibre content was calculated as follows:

Crude fibre (%) = [(mass of dried residue − mass of ash after incineration) / initial sample mass] × 100

Total carbohydrate content was estimated by difference using the following equation:

Carbohydrates (%) = 100 − [moisture (%) + ash (%) + crude protein (%) + crude lipid (%) + crude fibre (%)]

For mineral analysis, approximately 0.50 g of the dried and homogenized seaweed powder was transferred to a digestion vessel and mixed with 8 mL of concentrated nitric acid and 2 mL of hydrogen peroxide. Samples were digested using a closed-vessel microwave digestion system following a validated procedure for organic and siliceous matrices (US 1996). After cooling, the digests were quantitatively transferred to 50-mL volumetric flasks and brought to volume with ultrapure water.

Phosphorus was determined using the molybdenum-blue colorimetric method and quantified spectrophotometrically against prepared phosphorus standards. Potassium and sodium were

quantified using flame photometry, while calcium and magnesium were measured by atomic absorption spectrometry. Alternatively, all mineral elements may be quantified simultaneously by inductively coupled plasma–optical emission spectrometry if this instrument was used. Total nitrogen was determined by the Kjeldahl method described above.

Calibration curves were constructed using certified elemental standards. Reagent blanks and, where available, certified reference materials were included to assess contamination, analytical accuracy, and recovery. Mineral concentrations were expressed as g kg^{-1} dry weight.

Nanoparticle characterization

X-ray diffraction (XRD)

The crystalline structure and phase composition of MNS and Nano-Fe particles were characterized using XRD analysis. Powdered nanoparticle samples were dried at room temperature and finely ground prior to analysis. XRD patterns were recorded using an X-ray diffractometer equipped with Cu-Kα radiation (λ = 1.5406 Å) operating at 40 kV and 30 mA. Diffraction data were collected over a 2θ range of 5–80° with a scanning rate of 2° min^{-1} and a step size of 0.02°. The obtained diffraction peaks were compared with standard JCPDS reference files to identify the crystalline phases and confirm nanoparticle formation. Crystallite size was estimated using the Scherrer equation based on the full width at half maximum (FWHM) of the dominant diffraction peaks.

Fourier transform infrared spectroscopy (FTIR)

FTIR analysis was performed to identify the functional groups and chemical bonding characteristics of the synthesized nanoparticles. Dried nanoparticle samples were mixed with potassium bromide (KBr) powder and compressed into translucent pellets under hydraulic pressure. FTIR spectra were recorded using an FTIR spectrometer within the wavenumber range of 4000–400 cm^{-1} at a spectral resolution of 4 cm^{-1}. The spectra were analyzed to identify characteristic absorption bands corresponding to hydroxyl, silanol, Fe–O, Si–O–Si, and other surface functional groups involved in nanoparticle stabilization and interaction. Changes in peak intensity and band shifts were used to evaluate the chemical structure and surface properties of the nanoparticles.

Dynamic light scattering (DLS)

The hydrodynamic particle size distribution and polydispersity index (PDI) of mesoporous nano-silica and nano-iron suspensions were determined using DLS analysis. Nanoparticle samples were dispersed in deionized water and ultrasonicated for 20 min to minimize aggregation and obtain homogeneous suspensions. Measurements were conducted using a particle size analyzer equipped with a laser light source operating at 25 °C. The average hydrodynamic diameter, particle size distribution, and PDI values were recorded from three independent measurements for each sample. The obtained data were used to evaluate nanoparticle dispersion stability and uniformity in aqueous suspension prior to foliar application.

Lipid peroxidation (MDA)

Lipid peroxidation was determined by MDA content according to the method of Heath and Packer with slight modifications. Fresh leaf tissue (0.5 g) was homogenized in 5 mL of 0.1% (w/v) trichloroacetic acid (TCA) using a chilled mortar and pestle. The homogenate was centrifuged at 10,000 ×g for 10 min at 4 °C. Subsequently, 1 mL of the supernatant was mixed with 4 mL of 20% TCA containing 0.5% thiobarbituric acid (TBA). The reaction mixture was heated at 95 °C for 30 min and then rapidly cooled in an ice bath to terminate the reaction. After centrifugation at 10,000 ×g for 10 min, the absorbance of the supernatant was recorded at 532 and 600 nm using a UV–Vis spectrophotometer. The nonspecific absorbance at 600 nm was subtracted from the absorbance at 532 nm, and MDA concentration was calculated using an extinction coefficient of 155 mM^{-1} cm^{-1} and expressed as nmol g^{-1} fresh weight (FW) (Heath and Packer 1968).

Proline content

Free proline content was quantified following the method described by Bates et al. Fresh leaf tissue (0.5 g) was homogenized in 10 mL of 3% sulfosalicylic acid and filtered through Whatman No. 2 filter paper. Two milliliters of the filtrate were mixed with 2 mL of acid ninhydrin reagent and 2 mL of glacial acetic acid in a test tube. The reaction mixture was incubated at 100 °C for 1 h in a water bath and subsequently cooled in an ice bath. The chromophore was extracted with 4 mL toluene, and the absorbance of the upper organic phase was measured at 520 nm. Proline concentration was determined using a standard calibration curve and expressed as μmol g^{-1} FW (Bates et al. 1973).

Hydrogen peroxide (H_2O_2)

H_2O_2 content was determined according to the method of Velikova et al. Fresh leaf tissue (0.5 g) was homogenized in 5 mL of cold 0.1% TCA and centrifuged at 12,000 ×g for 15 min at 4 °C. The reaction mixture contained 0.5 mL of supernatant, 0.5 mL of 10 mM potassium phosphate buffer (pH 7.0), and 1 mL of 1 M potassium iodide (KI). The absorbance was measured at 390 nm using a spectrophotometer. H_2O_2 concentration was calculated using a standard curve prepared with known concentrations of H_2O_2 and expressed as μmol g^{-1} FW (Velikova et al. 2000).

Soluble protein content

Total soluble protein content was determined according to the method of Bradford using bovine serum albumin (BSA) as the standard. Fresh leaf tissue (0.5 g) was homogenized in 5 mL of phosphate buffer (50 mM, pH 7.0) and centrifuged at 12,000 ×g for 15 min at 4 °C. An aliquot of 0.1 mL of the supernatant was mixed with 5 mL of Bradford reagent and incubated at room temperature for 10 min. The absorbance was measured at 595 nm using a UV–Vis spectrophotometer. Protein concentration was calculated from a BSA standard curve and expressed as mg g^{-1} FW (Bradford 1976).

Antioxidant enzyme extraction

For antioxidant enzyme assays, fresh leaf samples (0.5 g) were homogenized in 5 mL of ice-cold extraction buffer containing 50 mM potassium phosphate buffer (pH 7.0), 1 mM ethylenediaminetetraacetic acid (EDTA), 1% polyvinylpyrrolidone (PVP), and 0.1 mM phenylmethylsulfonyl fluoride (PMSF). The homogenate was centrifuged at 15,000 ×g for 20 min at 4 °C, and the supernatant was collected and used for enzyme activity determination. All extraction procedures were performed at 4 °C to minimize enzyme degradation.

Catalase (CAT)

CAT (EC 1.11.1.6) activity was determined according to the method of Aebi by monitoring the decomposition of hydrogen peroxide (H_2O_2). The reaction mixture contained 50 mM potassium phosphate buffer (pH 7.0), 15 mM H_2O_2, and enzyme extract in a final volume of 3 mL. The decrease in absorbance was recorded at 240 nm for 1 min using a UV–Vis spectrophotometer. CAT activity was calculated using the extinction coefficient of H_2O_2 (39.4 mM^{-1} cm^{-1}) and expressed as U mg^{-1} protein (Aebi 1984).

Superoxide dismutase (SOD)

SOD (EC 1.15.1.1) activity was measured according to the method of Giannopolitis and Ries based on the inhibition of nitro blue tetrazolium (NBT) photoreduction. The reaction mixture contained 50 mM phosphate buffer (pH 7.8), 13 mM methionine, 75 μM NBT, 2 μM riboflavin, 0.1 mM EDTA, and enzyme extract. The reaction tubes were illuminated under fluorescent light for 15 min, while a non-illuminated mixture served as the blank. Absorbance was measured at 560 nm. One unit of SOD activity was defined as the amount of enzyme causing 50% inhibition of NBT reduction and expressed as U mg^{-1} protein (Giannopolitis and Ries 1977).

Ascorbate peroxidase (APX)

APX (EC 1.11.1.11) activity was determined according to the method of Nakano and Asada by monitoring the oxidation of ascorbate. The reaction mixture contained 50 mM potassium phosphate buffer (pH 7.0), 0.5 mM ascorbic acid, 0.1 mM H_2O_2, 0.1 mM EDTA, and enzyme extract in a final volume of 3 mL. The decrease in absorbance was recorded at 290 nm for 1 min. APX activity was calculated using the extinction coefficient of ascorbate (2.8 mM^{-1} cm^{-1}) and expressed as U mg^{-1} protein (Nakano and Asada 1981).

Polyphenol oxidase (PPO)

PPO (EC 1.14.18.1) activity was measured following the method of Mayer nd Harel using catechol as the substrate. The reaction mixture consisted of 50 mM phosphate buffer (pH 6.5), 20 mM catechol, and enzyme extract in a final volume of 3 mL. The increase in absorbance due to catechol oxidation was monitored at 420 nm for 3 min. PPO activity was expressed as U mg^{-1} protein based on the change in absorbance per minute (Mayer and Harel 1979).

Photosynthetic pigments (chlorophyll and carotenoids)

Photosynthetic pigments including Chl a, Chl b, total chlorophyll, and carotenoids were determined according to the method of Lichtenthaler. Fresh leaf tissue (0.2 g) was homogenized in 10 mL of 80% acetone and centrifuged at 10,000 ×g for 10 min. The absorbance of the supernatant was measured at 663, 645, and 470 nm using a UV–Vis spectrophotometer. Pigment concentrations were calculated using the following equations:

- Chlorophyll a (Chl a) = 12.7 × A663 – 2.69 × A645

- Chlorophyll b (Chl b) = 22.9 × A645 – 4.68 × A663
- Total chlorophyll (Chl a + b) = 20.2 × A645 + 8.02 × A663
- Carotenoids = (1000 × A470 – 1.82 × Chl a – 85.02 × Chl b) / 198

Pigment contents were expressed as mg g^{-1} fresh weight (FW) (Lichtenthaler and Wellburn 1983).

Gas exchange measurements

Gas exchange parameters were measured on fully expanded young leaves using a portable photosynthesis system, such as LI-6400XT or LI-6800. Measurements were performed between 09:00 and 11:30 under stable greenhouse conditions. The leaf chamber was adjusted to a photosynthetic photon flux density of 1000–1200 μmol m^{-2} s^{-1}, reference CO_2 concentration of 400 μmol mol^{-1}, leaf temperature of 25 ± 2 °C, and relative humidity of approximately 60–70%. Net photosynthetic rate (Pn), stomatal conductance (gs), transpiration rate (E), and intercellular CO_2 concentration (Ci) were recorded after readings reached a steady state. Intrinsic water-use efficiency was calculated as the ratio of Pn to gs, while instantaneous water-use efficiency was calculated as the ratio of Pn to E. Measurements were taken from at least three plants per treatment and expressed on a leaf-area basis.

Mineral nutrient analysis

Mineral nutrient concentrations were determined in dried leaf samples collected at the end of the experiment. Plant samples were initially washed with tap water followed by distilled water to remove surface contaminants, then oven-dried at 70 °C until constant weight and finely ground (Jones 1991). Approximately 0.5 g of dried plant material was digested using a concentrated sulfuric acid–hydrogen peroxide or nitric acid–perchloric acid digestion mixture until a clear solution was obtained (Pratt and Chapman 1961). After cooling, the digested extract was filtered and diluted to a known final volume with distilled water.

Sodium (Na^+), potassium (K^+), and calcium (Ca^{2+}) concentrations were quantified using a flame photometer or atomic absorption spectrophotometer (Jones 1991). Iron (Fe), silicon (Si), zinc (Zn), magnesium (Mg), and other micronutrients were determined using atomic absorption spectroscopy or inductively coupled plasma optical emission spectroscopy (Wolf, 1982). Phosphorus (P) concentration was measured colorimetrically using the molybdenum blue method (Murphy and

Riley 1962), while nitrogen (N) was determined by the Kjeldahl method (Bremner 1965). Chloride (Cl^-) concentration was measured by silver nitrate titration or ion chromatography following aqueous extraction of dried tissues. The Na^+/Cl^- ratio was subsequently calculated to evaluate ionic balance and salinity tolerance under salt stress conditions. Macronutrient concentrations were expressed as mg g^{-1} dry weight (DW), whereas micronutrient concentrations were expressed as mg kg^{-1} DW.

Expression of stress-responsive genes

The relative expression levels of selected stress-responsive genes in maize leaves were analyzed using quantitative real-time PCR (qRT-PCR) following standard molecular biology protocols (Bustin et al. 2009). Fresh leaf samples were collected from each treatment at the end of the experimental period, immediately frozen in liquid nitrogen, and stored at −80 °C until RNA extraction. Total RNA was extracted from approximately 100 mg of frozen leaf tissue using an appropriate plant RNA extraction kit according to the manufacturer's instructions (Ghawana et al. 2011). The quality and concentration of extracted RNA were assessed using a spectrophotometer based on absorbance at 260 and 280 nm. RNA integrity was also checked by agarose gel electrophoresis. To eliminate genomic DNA contamination, RNA samples were treated with DNase I prior to cDNA synthesis (Bustin et al. 2009). First-strand cDNA was synthesized from purified RNA using a reverse transcription kit following the manufacturer's protocol. The synthesized cDNA was diluted to the appropriate concentration and used as a template for qRT-PCR analysis. Gene-specific primers were designed for selected stress-responsive genes, including *ZmDREB2A*, *ZmHSP70*, *ZmP5CS*, *ZmCAT1*, and *ZmNHX1*.

Quantitative real-time PCR was performed using SYBR Green PCR master mix in a real-time PCR detection system (Bustin et al. 2009). Each reaction mixture contained SYBR Green master mix, forward and reverse primers, cDNA template, and nuclease-free water. The amplification program consisted of an initial denaturation step, followed by 40 amplification cycles of denaturation, annealing, and extension. Melting curve analysis was performed at the end of the amplification cycles to confirm primer specificity and the absence of non-specific products.

The maize actin gene was used as the internal reference gene for normalization of gene expression data. All reactions were carried out in three biological replicates with technical replication. Relative gene expression levels were calculated using the 2^−ΔΔCt method (Livak and Schmittgen 2001). The expression level of the non-saline untreated control was set as 1.0, and fold changes in gene expression were calculated relative to this control.

Statistical analysis

The experiment was conducted as a factorial completely randomized design (CRD) with three factors including salinity stress, nanoparticle treatment, and biostimulant application. All collected data were subjected to analysis of variance (ANOVA) using SAS software version 9.4 or SPSS version 25. The significance of the main effects and their interactions was evaluated at the 5% probability level ($p \leq 0.05$). Before statistical analysis, data normality and homogeneity of variance were examined using the Shapiro–Wilk and Levene's tests, respectively.

When significant differences among treatments were observed, mean comparisons were performed using the least significant difference (LSD) test at $p \leq 0.05$. All measurements were conducted with four biological replicates, and the obtained results were expressed as mean ± standard error (SE). Additionally, Pearson correlation analysis was performed to investigate the relationships among physiological, biochemical, antioxidant, and mineral nutrient traits under salinity stress conditions. Principal component analysis (PCA) and hierarchical clustering heatmap analysis were also carried out to identify the most responsive variables and evaluate treatment discrimination patterns associated with salinity tolerance in maize plants.

Result

Structural and physicochemical characterization of the nanoparticles

The XRD patterns revealed distinct diffraction profiles for MNS and Nano-Fe. MNS exhibited a broad dominant maximum at approximately $2\theta = 13°$, accompanied by weaker maxima near 27°, 39°, 50°, and 67° (Figure 1A). In contrast, Nano-Fe displayed sharper reflections, with the

strongest peak located near 34° and additional peaks at approximately 24°, 38°, 54°, 61°, and 70° (Figure 1B).

The FTIR spectrum of MNS showed a broad absorption band centred at approximately 3440 cm^{-1}, assigned to O–H stretching, and a band at 1635 cm^{-1} associated with H–O–H bending. The prominent absorption at 1090 cm^{-1}, together with bands at 803 and 465 cm^{-1}, corresponded to asymmetric Si–O–Si stretching, symmetric Si–O–Si stretching, and Si–O bending, respectively (Figure 1C). For Nano-Fe, bands at approximately 3430 and 1630 cm^{-1} were associated with hydroxyl groups and adsorbed water, whereas absorptions at 586 and 470 cm^{-1} were assigned to Fe–O vibrations (Figure 1D).

DLS analysis showed a single predominant intensity-weighted size population for each suspension. The reported Z-average hydrodynamic diameters were 120.6 ± 3.8 nm for MNS and 78.4 ± 2.6 nm for Nano-Fe, with corresponding polydispersity indices of 0.186 ± 0.02 and 0.162 ± 0.01 (Figure 1E, F). Thus, Nano-Fe had a lower reported hydrodynamic diameter and polydispersity index than MNS. The correlation-function intercepts were 0.91 and 0.93, respectively.

Morphological traits

Salinity stress significantly reduced all measured morphological traits of maize plants, including plant height, fresh weight, dry weight, and number of leaves, whereas the application of MNS, Nano-Fe, and ANE, either individually or in combination, markedly improved plant growth under both normal and saline conditions (Table 3). Under non-saline conditions (0 mM NaCl), the combined application of MNS + Nano-Fe + ANE produced the highest growth performance among all treatments. Plant height increased to 81.30 cm compared with 69.25 cm in the untreated control, representing an increase of approximately 17.4%. Similarly, fresh and dry biomass increased substantially, reaching 59.75 and 17.45 g $plant^{-1}$, respectively, compared with 46.85 and 12.80 g $plant^{-1}$ in the control plants. The number of leaves also increased from 29.40 leaves $plant^{-1}$ in the control to 38.60 leaves $plant^{-1}$ following combined nanoparticle and biostimulant application. The dual combinations, particularly MNS + Nano-Fe and Nano-Fe + ANE, also significantly enhanced morphological performance relative to individual treatments.

Moderate salinity stress (75 mM NaCl) markedly suppressed maize growth, as indicated by reductions in plant height, biomass accumulation, and leaf number in untreated plants. Plant height declined from 69.25 cm under non-saline control conditions to 54.40 cm under salinity stress alone, while fresh and dry weights decreased by approximately 29.2% and 30.1%, respectively. However, nanoparticle and biostimulant applications effectively alleviated these inhibitory effects. The MNS + Nano-Fe + ANE treatment exhibited the greatest mitigation capacity, increasing plant height, fresh weight, dry weight, and leaf number to 68.40 cm, 46.55 g plant^{-1}, 13.55 g plant^{-1}, and 32.10 leaves plant^{-1}, respectively. These values were substantially higher than those recorded for salinity-stressed control plants and approached the values observed under non-saline conditions (Table 3).

Severe salinity stress (150 mM NaCl) caused pronounced growth inhibition in maize plants. Untreated stressed plants exhibited the lowest values for all morphological parameters, with plant height decreasing to 39.15 cm, fresh weight to 21.45 g plant^{-1}, dry weight to 5.35 g plant^{-1}, and number of leaves to 15.60 leaves plant^{-1}. Nevertheless, the combined nanoparticle–biostimulant treatments significantly improved plant performance under severe salinity. Among all treatments, MNS + Nano-Fe + ANE showed the strongest protective effect, increasing plant height by approximately 47.8%, fresh weight by 72.0%, dry weight by 101.9%, and leaf number by 72.8% relative to salinity-stressed control plants. Individual applications of MNS, Nano-Fe, or ANE also improved growth traits compared with untreated stressed plants, although their effects were less pronounced than those of combined treatments (Table 3).

Lipid peroxidation

Salinity stress significantly increased lipid peroxidation in maize plants, as evidenced by elevated MDA accumulation (Figure 2A). The highest MDA content was observed in untreated plants exposed to severe salinity (150 mM NaCl), reaching 7.25 nmol g^{-1} FW, compared with only 2.18 nmol g^{-1} FW under non-saline control conditions. Application of MNS, Nano-Fe, and ANE, either individually or in combination, significantly reduced MDA accumulation under salinity stress. Among all treatments, the combined application of MNS + Nano-Fe + ANE showed the strongest protective effect, reducing MDA content to 3.95 nmol g^{-1} FW under severe salinity, representing a reduction of approximately 45.5% relative to untreated stressed plants. Dual combinations such as MNS + Nano-Fe and Nano-Fe + ANE also markedly lowered MDA levels compared with salinity-stressed controls, indicating reduced membrane lipid peroxidation and oxidative damage.

Proline accumulation

Proline accumulation increased progressively with increasing salinity levels and was further enhanced by nanoparticle and biostimulant treatments. Under severe salinity stress, untreated plants accumulated 7.10 µmol g^{-1} FW proline, whereas plants receiving MNS + Nano-Fe + ANE exhibited the highest proline content of 8.85 µmol g^{-1} FW. Individual applications of Nano-Fe, MNS, and ANE also increased proline accumulation relative to untreated stressed plants. Under moderate salinity (75 mM NaCl), the combined treatment significantly enhanced proline accumulation to 6.05 µmol g^{-1} FW compared with 4.15 µmol g^{-1} FW in stressed control plants (Figure 2B).

Hydrogen peroxide

H_2O_2 concentration increased substantially under salinity stress, indicating enhanced oxidative stress in maize plants. The highest H_2O_2 content was recorded in untreated plants exposed to 150 mM NaCl (10.25 µmol g^{-1} FW), whereas non-saline control plants exhibited only 3.35 µmol g^{-1} FW. The application of nanoparticles and ANE significantly reduced H_2O_2 accumulation under both moderate and severe salinity conditions. The greatest reduction was observed in plants treated with MNS + Nano-Fe + ANE, where H_2O_2 levels decreased to 5.90 µmol g^{-1} FW under severe salinity stress. Similarly, MNS + Nano-Fe and Nano-Fe + ANE treatments substantially lowered H_2O_2 accumulation compared with untreated stressed plants (Figure 2C).

Soluble protein content

Soluble protein content declined markedly with increasing salinity stress, whereas nanoparticle and biostimulant applications significantly improved protein accumulation (Figure 2D). Severe salinity reduced soluble protein content from 22.80 mg g^{-1} FW in the non-saline control to 14.25 mg g^{-1} FW in untreated stressed plants. However, application of MNS, Nano-Fe, and ANE alleviated these reductions and enhanced protein synthesis under stress conditions. The highest soluble protein content under severe salinity was recorded in plants treated with MNS + Nano-Fe + ANE (22.55 mg g^{-1} FW), followed by MNS + Nano-Fe (20.80 mg g^{-1} FW). Under non-saline conditions, combined treatments also enhanced protein accumulation compared with untreated control plants.

Catalase

CAT activity increased significantly in response to salinity stress, indicating enhanced activation of the antioxidant defense system in maize plants (Figure 3A). In untreated plants, CAT activity increased from 18.45 U mg^{-1} protein under non-saline conditions to 48.20 U mg^{-1} protein at 150 mM NaCl. The application of different nanoparticle and biostimulant treatments further influenced CAT activity depending on salinity level. Under moderate salinity stress (75 mM NaCl), the combined treatment of MNS + Nano-Fe + ANE markedly increased CAT activity to 45.60 U mg^{-1} protein compared with 31.40 U mg^{-1} protein in untreated stressed plants. Under severe salinity stress (150 mM NaCl), however, CAT activity in plants treated with MNS + Nano-Fe + ANE decreased to 46.50 U mg^{-1} protein relative to the untreated stressed control, although it remained substantially higher than the non-saline control plants.

Superoxide dismutase

SOD activity was strongly induced by salinity stress and was further modulated by nanoparticle and biostimulant treatments (Figure 3B). In untreated plants, SOD activity increased markedly from 62.80 U mg^{-1} protein under non-saline conditions to 140.85 U mg^{-1} protein under severe salinity stress (150 mM NaCl), reflecting enhanced oxidative stress. Application of MNS, Nano-Fe, ANE, and their combinations altered SOD activity depending on salinity intensity. Under moderate salinity stress (75 mM NaCl), the highest SOD activity was observed in plants treated with Nano-Fe (134.50 U mg^{-1} protein), followed by MNS + Nano-Fe (122.60 U mg^{-1} protein) and Nano-Fe + ANE (118.40 U mg^{-1} protein). Under severe salinity stress, untreated plants still exhibited the highest SOD activity, whereas combined treatments generally reduced enzyme activity compared with the stressed control.

Ascorbate peroxidase

APX activity increased progressively with increasing salinity stress, indicating enhanced activation of the antioxidant defense system in maize plants (Figure 3C). In untreated plants, APX activity increased from 5.60 U mg^{-1} protein under non-saline conditions to 18.20 U mg^{-1} protein under severe salinity stress (150 mM NaCl). The application of MNS, Nano-Fe, ANE, and their combinations further modulated APX activity under saline conditions. Under moderate salinity stress (75 mM NaCl), the combined treatment of MNS + Nano-Fe + ANE resulted in the highest

APX activity (23.30 U mg^{-1} protein), followed by Nano-Fe + ANE (18.65 U mg^{-1} protein) and MNS + Nano-Fe (17.10 U mg^{-1} protein). Under severe salinity stress, the MNS + Nano-Fe + ANE treatment maintained a high APX activity (22.30 U mg^{-1} protein), exceeding that of untreated stressed plants (18.20 U mg^{-1} protein).

Polyphenol oxidase

PPO activity was significantly affected by salinity stress and nanoparticle biostimulant applications (Figure 3D). In untreated plants, PPO activity increased from 5.10 U mg^{-1} protein under non-saline conditions to 10.95 U mg^{-1} protein under severe salinity stress (150 mM NaCl), indicating enhanced oxidative stress responses. Application of MNS, Nano-Fe, ANE, and their combined treatments further influenced PPO activity under saline conditions. Under moderate salinity stress (75 mM NaCl), the highest PPO activity was observed in plants treated with MNS + Nano-Fe + ANE (14.63 U mg^{-1} protein), followed by MNS + Nano-Fe (11.65 U mg^{-1} protein) and Nano-Fe + ANE (11.20 U mg^{-1} protein). Under severe salinity stress, Nano-Fe + ANE treatment produced the highest PPO activity (14.02 U mg^{-1} protein), whereas MNS + Nano-Fe reduced PPO activity to 10.80 U mg^{-1} protein relative to the untreated stressed control.

Chlorophyll a

Salinity stress significantly reduced Chlo a content in maize plants, whereas nanoparticle and biostimulant treatments alleviated pigment degradation and improved Chlo accumulation (Table 4). Under severe salinity stress (150 mM NaCl), Chlo a content declined markedly from 1.92 mg g^{-1} FW in non-saline control plants to 0.98 mg g^{-1} FW in untreated stressed plants, representing a reduction of approximately 49.0%. Application of MNS + Nano-Fe + ANE, either individually or in combination, significantly enhanced Chlo a content under saline conditions. The greatest improvement was observed in plants treated with MNS + Nano-Fe + ANE, where Chlo a increased to 1.72 mg g^{-1} FW under severe salinity stress. Similarly, MNS + Nano-Fe and Nano-Fe + ANE treatments also maintained significantly higher Chlo a levels compared with untreated stressed plants. Under non-saline conditions, combined treatments enhanced Chlo a content beyond the untreated control, with the highest value (2.40 mg g^{-1} FW) recorded for MNS + Nano-Fe + ANE (Table 4).

Chlorophyll b

A similar trend was observed for Chlo b content. Salinity stress caused a substantial decline in Chlo b, decreasing from 0.75 mg g^{-1} FW in the non-saline control to 0.40 mg g^{-1} FW in plants subjected to severe salinity without treatment. However, nanoparticle and biostimulant applications significantly mitigated these reductions. The combined treatment of MNS + Nano-Fe + ANE produced the highest Chlo b content under severe salinity stress (0.72 mg g^{-1} FW), followed by MNS + Nano-Fe (0.66 mg g^{-1} FW). Moderate salinity stress also reduced Chlo b levels, although combined treatments effectively improved pigment retention relative to untreated stressed plants. Under non-saline conditions, the highest Chlo b content (0.98 mg g^{-1} FW) was recorded in plants receiving MNS + Nano-Fe + ANE (Table 4).

Total chlorophyll

Total Chlo content decreased progressively with increasing salinity levels, indicating salinity-induced impairment of the photosynthetic apparatus. Severe salinity stress reduced total Chlo content from 2.67 mg g^{-1} FW in control plants to 1.38 mg g^{-1} FW in untreated stressed plants. Nevertheless, application of nanoparticles and ANE significantly improved total Chlo accumulation under both moderate and severe salinity conditions. The MNS + Nano-Fe + ANE treatment showed the strongest protective effect, increasing total chlorophyll content to 2.44 mg g^{-1} FW under severe salinity stress, corresponding to an increase of approximately 76.8% relative to untreated stressed plants. Likewise, MNS + Nano-Fe and Nano-Fe + ANE treatments also maintained significantly higher Chlo contents than untreated stressed plants. Under optimal conditions, the highest total chlorophyll value (3.38 mg g^{-1} FW) was observed in plants treated with MNS + Nano-Fe + ANE (Table 4).

Carotenoids

Carotenoid content was also significantly influenced by salinity stress and nanoparticle–biostimulant treatments (Table 4). Untreated plants exposed to severe salinity exhibited the lowest carotenoid content (0.31 mg g^{-1} FW), whereas non-saline control plants maintained 0.60 mg g^{-1} FW. The application of MNS, Nano-Fe, and ANE effectively enhanced carotenoid accumulation under salinity stress, particularly when applied in combination. Plants treated with MNS + Nano-Fe + ANE showed the highest carotenoid content under severe salinity stress (0.58 mg g^{-1} FW),

followed by MNS + Nano-Fe (0.52 mg g^{-1} FW). Similar improvements were observed under moderate salinity stress. Under non-saline conditions, combined nanoparticle and biostimulant application produced the highest carotenoid accumulation (0.79 mg g^{-1} FW).

Nitrogen

Salinity stress significantly reduced N accumulation in maize plants, whereas the application of MNS + Nano-Fe + ANE improved N uptake under both normal and saline conditions (Figure 4A). Under severe salinity stress (150 mM NaCl), untreated plants exhibited the lowest N content (17.20 mg g^{-1} DW), compared with 28.80 mg g^{-1} DW under non-saline control conditions. The combined application of MNS + Nano-Fe + ANE markedly alleviated salinity-induced reductions in N content, increasing it to 27.90 mg g^{-1} DW under severe salinity stress. Similarly, MNS + Nano-Fe and Nano-Fe + ANE treatments significantly improved N accumulation relative to untreated stressed plants. Under non-saline conditions, the highest N concentration (34.75 mg g^{-1} DW) was recorded in plants treated with MNS + Nano-Fe + ANE.

Phosphorus

P content decreased progressively with increasing salinity stress levels. Severe salinity reduced P concentration from 3.30 mg g^{-1} DW in the non-saline control to 1.82 mg g^{-1} DW in untreated stressed plants. However, nanoparticle and biostimulant applications significantly enhanced phosphorus uptake under salinity conditions. The highest P concentration under severe salinity stress was observed in plants treated with MNS + Nano-Fe + ANE (3.15 mg g^{-1} DW), followed by MNS + Nano-Fe (2.85 mg g^{-1} DW). Moderate salinity stress also reduced P accumulation, although combined treatments effectively improved phosphorus content compared with untreated stressed plants. Under optimal conditions, MNS + Nano-Fe + ANE treatment produced the highest phosphorus concentration (4.12 mg g^{-1} DW) (Figure 4B).

Potassium

K content was significantly affected by salinity stress and nanoparticle–biostimulant treatments. Salinity markedly reduced K accumulation in maize plants, with untreated plants exposed to severe salinity exhibiting the lowest K content (19.95 mg g^{-1} DW). In contrast, integrated nanoparticle and ANE applications substantially improved potassium accumulation under saline conditions. The combined treatment of MNS + Nano-Fe + ANE increased K content to 33.10 mg g^{-1} DW

under severe salinity stress, representing an increase of approximately 65.9% relative to untreated stressed plants. Similar improvements were observed with MNS + Nano-Fe and Nano-Fe + ANE treatments. Under non-saline conditions, the highest K concentration (41.60 mg g^{-1} DW) was recorded in plants receiving the combined MNS + Nano-Fe + ANE treatment (Figure 4AC).

Calcium

Ca accumulation significantly declined with increasing salinity stress. Severe salinity stress reduced Ca content from 15.45 mg g^{-1} DW in non-saline control plants to 9.45 mg g^{-1} DW in untreated stressed plants. Nevertheless, the application of MNS, Nano-Fe, and ANE significantly enhanced calcium uptake under saline conditions. The highest Ca concentration under severe salinity stress was observed in plants treated with MNS + Nano-Fe + ANE (15.75 mg g^{-1} DW), followed by MNS + Nano-Fe (14.20 mg g^{-1} DW) (Figure 4D).

Silicon

Si concentration was strongly influenced by MNS application and salinity stress (Figure 4E). Untreated plants exposed to severe salinity stress exhibited the lowest Si content (0.62 mg g^{-1} DW), whereas treatments containing MNS significantly enhanced silicon accumulation under all salinity levels. The highest Si concentration under severe salinity was observed in plants treated with MNS + Nano-Fe + ANE (2.95 mg g^{-1} DW), followed by MNS + Nano-Fe (2.65 mg g^{-1} DW). Similar trends were observed under moderate salinity and non-saline conditions. In contrast, treatments without MNS showed comparatively lower silicon accumulation.

Sodium

Salinity stress substantially increased Na accumulation in plant tissues across all treatments. In the untreated control, Na concentration increased sharply from 8.25 under non-saline conditions to 24.85 and 42.60 at 75 and 150 mM NaCl, respectively. Application of MNS + Nano-Fe + ANE reduced Na accumulation compared with the control under both salinity levels (Figure 5A). Among the individual treatments, NFe was more effective than MNS and ANE, recording Na values of 18.95 and 32.40 at 75 and 150 mM NaCl, respectively. The combined treatments produced greater reductions in Na content, particularly MNS+NFe and MNS+NFe+ANE. The lowest Na concentrations were observed in plants treated with MNS+NFe+ANE, which decreased Na accumulation to 13.60 and 24.75 under moderate and severe salinity, respectively.

Chloride

Cl accumulation also increased markedly with increasing salinity levels. In the control treatment, Cl concentration increased from 12.40 at 0 mM NaCl to 36.85 and 68.20 at 75 and 150 mM NaCl, respectively (Figure 5B). All applied treatments significantly reduced Cl accumulation compared with untreated plants. The combined treatments were more effective than individual applications in restricting Cl uptake. The MNS+NFe treatment reduced Cl concentration to 24.60 and 46.85 under 75 and 150 mM NaCl, respectively, while the combined MNS+NFe+ANE treatment showed the greatest reduction, with Cl values decreasing to 21.30 and 41.95 under moderate and severe salinity conditions, respectively.

Iron

Salinity stress significantly reduced Fe accumulation in maize plants, whereas MNS + Nano-Fe + ANE improved Fe uptake under both non-saline and saline conditions (Figure 6A). Severe salinity stress decreased Fe concentration from 86.40 mg kg^{-1} DW in the non-saline control to 56.40 mg kg^{-1} DW in untreated stressed plants. Application of Nano-Fe alone or in combination with other treatments substantially enhanced iron accumulation. The highest Fe concentration was recorded in plants treated with MNS + Nano-Fe + ANE under non-saline conditions (132.75 mg kg^{-1} DW), while under severe salinity stress the same treatment increased Fe content to 108.55 mg kg^{-1} DW, representing an increase of approximately 92.5% relative to untreated stressed plants.

Zinc

Zn concentration declined progressively with increasing salinity levels. Untreated plants exposed to severe salinity exhibited the lowest Zn content (22.85 mg kg^{-1} DW), whereas non-saline plants treated with MNS + Nano-Fe + ANE showed the highest Zn accumulation (50.40 mg kg^{-1} DW) (Figure 6B). Combined nanoparticle and biostimulant applications significantly enhanced Zn uptake under saline conditions compared with untreated stressed plants. Under severe salinity stress, MNS + Nano-Fe + ANE treatment increased Zn concentration to 40.85 mg kg^{-1} DW, while MNS + Nano-Fe and Nano-Fe + ANE also produced notable improvements. Moderate salinity stress caused smaller reductions in Zn concentration, although combined treatments effectively maintained higher Zn levels than untreated stressed plants.

Copper

Cu accumulation was significantly affected by salinity stress and nanoparticle–biostimulant applications (Figure 6C). Salinity stress markedly reduced Cu content from 9.25 mg kg^{-1} DW in the non-saline control to 5.95 mg kg^{-1} DW in untreated plants under severe salinity. However, application of MNS, Nano-Fe, and ANE significantly improved Cu accumulation under saline conditions. The highest Cu concentration under severe salinity stress was observed in plants treated with MNS + Nano-Fe + ANE (10.35 mg kg^{-1} DW), followed by MNS + Nano-Fe (9.40 mg kg^{-1} DW). Under non-saline conditions, the same combined treatment produced the maximum Cu concentration (12.85 mg kg^{-1} DW).

Manganese

Mn concentration also declined significantly under salinity stress. Severe salinity reduced Mn content from 43.20 mg kg^{-1} DW in control plants to 29.10 mg kg^{-1} DW in untreated stressed plants. Nevertheless, nanoparticle and ANE treatments significantly enhanced Mn accumulation under saline conditions (Figure 6D). The greatest improvement was observed in plants treated with MNS + Nano-Fe + ANE, which increased Mn concentration to 46.60 mg kg^{-1} DW under severe salinity stress. Similarly, MNS + Nano-Fe and Nano-Fe + ANE treatments markedly improved Mn accumulation relative to untreated stressed plants. Under non-saline conditions, the combined MNS + Nano-Fe + ANE treatment resulted in the highest Mn concentration (55.85 mg kg^{-1} DW).

Net photosynthetic rate

Salinity stress significantly reduced the Pn of maize plants, whereas MNS + Nano-Fe + ANE alleviated these reductions and improved photosynthetic performance (Table 5). Severe salinity stress (150 mM NaCl) reduced Pn from 18.45 µmol CO_2 m^{-2} s^{-1} in non-saline control plants to 7.25 µmol CO_2 m^{-2} s^{-1} in untreated stressed plants, representing a reduction of approximately 60.7%. Application of nanoparticles and ANE significantly improved photosynthetic activity under saline conditions. The highest Pn under severe salinity was observed in plants treated with MNS + Nano-Fe + ANE (17.80 µmol CO_2 m^{-2} s^{-1}), followed by MNS + Nano-Fe (14.95 µmol CO_2 m^{-2} s^{-1}). Under non-saline conditions, combined application of MNS + Nano-Fe + ANE produced the highest photosynthetic rate (27.45 µmol CO_2 m^{-2} s^{-1}).

Stomatal conductance

Stomatal conductance declined markedly with increasing salinity stress levels. Untreated plants subjected to severe salinity exhibited the lowest gs value (0.16 mol H_2O m^{-2} s^{-1}), compared with 0.42 mol H_2O m^{-2} s^{-1} under non-saline control conditions. However, nanoparticle and ANE applications significantly improved stomatal conductance under saline conditions (Table 5). The combined treatment of MNS + Nano-Fe + ANE increased gs to 0.40 mol H_2O m^{-2} s^{-1} under severe salinity stress, while MNS + Nano-Fe and Nano-Fe + ANE treatments also significantly enhanced stomatal conductance compared with untreated stressed plants. Under moderate salinity stress, combined treatments similarly maintained higher gs values relative to the salinity-stressed control.

Transpiration rate

E was significantly suppressed by salinity stress, whereas nanoparticle and biostimulant applications effectively improved transpiration under saline conditions. Severe salinity reduced E from 5.85 mmol H_2O m^{-2} s^{-1} in the non-saline control to 2.35 mmol H_2O m^{-2} s^{-1} in untreated stressed plants. Nevertheless, combined treatments substantially mitigated these reductions. The MNS + Nano-Fe + ANE treatment increased transpiration rate to 5.55 mmol H_2O m^{-2} s^{-1} under severe salinity stress, followed by MNS + Nano-Fe (4.80 mmol H_2O m^{-2} s^{-1}) (Table 5). Similar trends were observed under moderate salinity conditions. Under non-saline conditions, the highest transpiration rate (8.10 mmol H_2O m^{-2} s^{-1}) was recorded in plants treated with MNS + Nano-Fe + ANE.

Intercellular CO_2 concentration

Ci decreased significantly under salinity stress but was markedly improved following nanoparticle and ANE application (Table 5). Untreated plants exposed to severe salinity stress showed the lowest Ci value (162.80 µmol mol^{-1}), whereas non-saline control plants maintained 268.40 µmol mol^{-1}. The integrated application of MNS + Nano-Fe + ANE significantly enhanced Ci under severe salinity stress, increasing it to 258.80 µmol mol^{-1}. Similarly, MNS + Nano-Fe and Nano-Fe + ANE treatments also improved intercellular CO_2 concentration compared with untreated stressed plants. Under non-saline conditions, the highest Ci value (312.80 µmol mol^{-1}) was observed in plants treated with MNS + Nano-Fe + ANE.

Expression of stress-responsive genes

Salinity stress markedly altered the expression patterns of stress-responsive genes in maize plants, while the application of MNS + Nano-Fe + ANE, either individually or in combination, significantly modulated transcriptional responses (Table 6). The relative expression levels of *ZmDREB2A*, *ZmHSP70*, *ZmP5CS*, *ZmCAT1*, and *ZmNHX1* increased progressively with increasing salinity intensity, indicating activation of osmotic adjustment, antioxidant defense, and ion homeostasis pathways.

Under moderate salinity stress (75 mM NaCl), the untreated control plants exhibited significant upregulation of all studied genes compared with the non-saline control. The expression of *ZmDREB2A*, *ZmHSP70*, and *ZmNHX1* increased to 3.85-, 4.10-, and 4.45-fold, respectively. However, plants treated with MNS, Nano-Fe, or ANE showed further enhancement of gene expression, particularly when treatments were combined. The combined treatment of MNS + Nano-Fe + ANE produced the highest transcript accumulation under 75 mM salinity, reaching 7.45-fold for *ZmDREB2A*, 8.10-fold for *ZmHSP70*, 8.42-fold for *ZmP5CS*, 7.35-fold for *ZmCAT1*, and 8.85-fold for *ZmNHX1*. These values were significantly greater than those recorded in untreated salt-stressed plants (Table 6).

Severe salinity stress (150 mM NaCl) further intensified stress-related gene expression in untreated plants, where *ZmNHX1* and *ZmP5CS* exhibited the greatest induction levels, reaching 10.45- and 9.75-fold, respectively. Similarly, *ZmDREB2A*, *ZmHSP70*, and *ZmCAT1* were strongly upregulated under severe stress conditions. Nevertheless, nano-enabled and biostimulant treatments moderated the excessive stress-induced transcriptional responses. Among the tested treatments, the combined application of MNS + Nano-Fe + ANE significantly reduced the overexpression of stress-related genes compared with untreated severely stressed plants, suggesting improved stress mitigation and cellular homeostasis. In this treatment, transcript levels decreased to 5.10-fold for *ZmDREB2A*, 5.55-fold for *ZmHSP70*, 5.85-fold for *ZmP5CS*, 5.02-fold for *ZmCAT1*, and 6.20-fold for *ZmNHX1* (Table 6).

Correlation analysis

Pearson correlation analysis revealed strong relationships among oxidative stress markers, antioxidant defense systems, photosynthetic pigments, and gas exchange parameters in maize plants exposed to salinity stress and nanoparticle–biostimulant treatments (Figure 7). MDA and H_2O_2 exhibited strong positive correlations with each other ($r = 0.93$), indicating coordinated

oxidative damage under salinity stress conditions. Both MDA and H_2O_2 showed pronounced negative correlations with chlorophyll pigments, gas exchange traits, and protein content. In particular, MDA was negatively correlated with Chlo a ($r = -0.76$), total Chlo ($r = -0.77$), Pn ($r = -0.80$), gs ($r = -0.77$), and E ($r = -0.73$), demonstrating the detrimental impact of oxidative stress on photosynthetic performance and cellular metabolism.

Proline accumulation displayed positive correlations with antioxidant enzymes including CAT ($r = 0.69$), SOD ($r = 0.73$), and APX ($r = 0.65$), suggesting that osmotic adjustment was closely associated with enhanced antioxidant defense under salinity stress. Similarly, CAT and SOD activities showed a very strong positive correlation ($r = 0.95$), reflecting the coordinated activation of enzymatic antioxidant systems in response to ROS accumulation. APX also exhibited strong positive associations with CAT ($r = 0.86$) and SOD ($r = 0.87$), indicating synergistic regulation among antioxidant enzymes.

Photosynthetic pigments were highly and positively correlated with gas exchange parameters. Chlorophyll a exhibited strong positive correlations with total chlorophyll ($r = 0.97$), Pn ($r = 0.93$), gs ($r = 0.90$), and E ($r = 0.88$), indicating that maintenance of pigment stability contributed directly to improved photosynthetic efficiency under stress conditions. Likewise, total chlorophyll was strongly correlated with Pn ($r = 0.94$) and gs ($r = 0.91$). Carotenoids also showed positive correlations with chlorophyll content and gas exchange traits, emphasizing their protective role against oxidative damage and photoinhibition.

PPO activity exhibited negative correlations with Chlo pigments and photosynthetic parameters, including Chlo a ($r = -0.72$), total Chlo ($r = -0.75$), and Pn ($r = -0.73$), suggesting that elevated PPO activity was associated with stress-induced metabolic disturbances and pigment degradation. In contrast, soluble protein content was positively correlated with photosynthetic pigments and gas exchange traits, particularly total Chlo ($r = 0.89$) and Pn ($r = 0.86$), indicating improved metabolic stability in nanoparticle- and biostimulant-treated plants.

Discussion

Salinity stress is considered one of the most detrimental abiotic stresses limiting plant productivity through osmotic imbalance, ionic toxicity, oxidative damage, nutrient disruption, impairment of

photosynthetic machinery, and metabolic dysfunction. In the present study, increasing NaCl concentrations markedly reduced maize growth, biomass accumulation, photosynthetic pigments, gas exchange performance, nutrient uptake, and physiological stability, while simultaneously increasing oxidative stress markers and altering antioxidant defense responses. However, the integrated application of MNS + Nano-Fe + ANE substantially alleviated the harmful effects of salinity stress, demonstrating strong synergistic effects on physiological, biochemical, nutritional, antioxidant, and molecular processes.

The severe reduction in plant height, biomass accumulation, and leaf development under salinity stress was closely associated with osmotic stress and ionic toxicity caused by excessive Na^+ accumulation (Balasubramaniam et al. 2023). Salinity stress limits cell division and cell elongation by reducing water uptake, disturbing membrane integrity, and impairing metabolic activity, ultimately suppressing plant growth and development (Shahid et al. 2020). The observed enhancement in morphological traits following MNS, Nano-Fe, and ANE application indicates that these treatments improved cellular hydration, nutrient acquisition, membrane stability, and metabolic performance under saline conditions (Farajollahi et al. 2023; Weisany and Khosropour 2023). Mesoporous nano-silica likely enhanced structural rigidity and membrane stability through silicon deposition in epidermal tissues, thereby reducing water loss and maintaining cellular turgor (Wang et al. 2021). Silicon has also been reported to reduce Na^+ transport from roots to shoots while improving K^+ retention and ionic selectivity, which contributes to improved growth under saline environments (Yan et al. 2025; Weisany et al. 2024). Nano-Fe may have stimulated chloroplast development, respiration, enzymatic activity, and energy metabolism because of its essential role in electron transport and chlorophyll biosynthesis (El-Desouky et al. 2021). Meanwhile, *A. nodosum* extract contains phytohormones, amino acids, polysaccharides, betaines, vitamins, and osmoprotective compounds that stimulate root development, nutrient absorption, osmotic adjustment, and stress-responsive signaling pathways (Kumari et al. 2023). The superior performance of the combined treatments suggests strong synergistic interactions among silicon-mediated membrane protection, iron-induced metabolic activation, and biostimulant-driven hormonal regulation.

The increase in MDA and H_2O_2 concentrations under salinity stress clearly indicated enhanced oxidative damage and membrane lipid peroxidation (Khan and Panda 2008). Salinity-induced

overproduction of ROS disrupts membrane permeability, protein stability, photosynthetic efficiency, and cellular metabolism (Hussain et al. 2021). The substantial reductions in MDA and H_2O_2 following nanoparticle and ANE application demonstrate the effectiveness of these treatments in controlling oxidative stress and protecting cellular structures (Tee et al. 2016). Silicon nanoparticles likely reduced ROS generation by stabilizing thylakoid membranes, preserving chloroplast ultrastructure, and improving antioxidant metabolism (Alam et al. 2022), whereas Nano-Fe may have enhanced ROS detoxification through its involvement in redox-active enzymes and electron transport systems (Soares et al. 2018). In addition, ANE contains phenolic compounds, betaines, alginates, antioxidant metabolites, and bioactive compounds capable of directly scavenging free radicals and stimulating stress-responsive defense pathways (Kumari et al. 2023). The strong reduction in oxidative markers observed in the combined treatments confirms that simultaneous improvement of antioxidant defense, nutrient balance, and membrane stability effectively mitigated salinity-induced oxidative injury.

Proline accumulation increased significantly under salinity stress and was further enhanced by nanoparticle and ANE treatments. Proline functions as an important osmoprotectant that stabilizes proteins, membranes, enzymes, and cellular osmotic potential under stress conditions (Singh et al. 2015). Enhanced proline accumulation in treated plants suggests improved osmotic adjustment, cellular hydration, and stress protection (Bhardwaj et al. 2025). ANE likely stimulated proline biosynthesis through hormonal and metabolic signaling pathways (Olaetxea et al. 2024), while Si and Fe nanoparticles may have enhanced amino acid metabolism and nitrogen assimilation, thereby supporting compatible solute accumulation (Koleva et al. 2022). Increased soluble protein content in treated plants further supports improved metabolic stability and protection against salinity-induced protein degradation and enzyme inactivation.

Salinity stress severely impaired chlorophyll accumulation and photosynthetic activity, which is commonly attributed to chloroplast damage, pigment degradation, stomatal closure, inhibition of photosynthetic enzymes, and disruption of photosystem functionality (Hussain et al. 2021). The decline in Chlo a, Chlo b, carotenoids, Pn, gs, E, and Ci in untreated stressed plants reflects substantial photosynthetic inhibition under saline conditions. The pronounced improvements observed following MNS, Nano-Fe, and ANE application indicate strong protection of the photosynthetic apparatus. Nano-Fe likely promoted chlorophyll biosynthesis due to its role in

ferredoxin formation, cytochrome activity, chloroplast electron transport, and enzymatic activation (Sepehrzadegan and Alizadeh 2021). Silicon nanoparticles may have improved chloroplast ultrastructure and enhanced stomatal regulation, thereby maintaining CO_2 diffusion and photosynthetic efficiency (Liang et al. 2023). The enhancement of carotenoids in treated plants also suggests improved photoprotection against ROS-mediated photooxidative damage (Li et al. 2026). Furthermore, ANE contains cytokinin-like compounds and bioactive metabolites capable of delaying chlorophyll degradation and sustaining photosynthetic metabolism under stress conditions (Minkov et al. 2026). The close correlation between pigment stability and gas exchange performance observed in the correlation analysis further confirms the coordinated regulation of photosynthesis and oxidative protection.

The improved macro- and micronutrient accumulation observed in treated plants represents another major mechanism underlying salinity tolerance. Salinity stress commonly reduces nutrient uptake because of ionic competition between Na^+ and essential nutrients such as K^+, Ca^{2+}, Mg^{2+}, and micronutrients (Awais et al. 2023). The marked improvement in N, P, K, Ca, Fe, Zn, Cu, Mn, and Si concentrations following nanoparticle and ANE application indicates enhanced nutrient acquisition, root activity, and ion homeostasis. Silicon likely reduced Na^+ toxicity and improved membrane selectivity, allowing greater uptake and transport of beneficial ions (Ali et al. 2021). Nano-Fe directly increased Fe availability and may have stimulated nutrient transporter activity, root metabolism, and enzymatic processes involved in nutrient assimilation (Abdulvawhab et al. 2026). In parallel, ANE probably enhanced root growth and rhizosphere activity through hormonal stimulation and organic compounds that improve nutrient mobilization and absorption (Minkov et al. 2026). Improved K^+ and Ca^{2+} accumulation is particularly important because these ions maintain membrane stability, osmotic regulation, enzyme activation, and stomatal functioning under saline conditions (Sardans and Peñuelas 2021).

The modulation of antioxidant enzyme activities further highlights the adaptive role of nanoparticle and biostimulant treatments in salinity tolerance. Increased CAT, SOD, APX, and PPO activities under salinity stress reflected activation of enzymatic ROS-scavenging systems (Mondal et al. 2023). However, the relatively lower antioxidant enzyme activities observed in severely stressed plants receiving combined treatments likely indicate reduced oxidative pressure due to more effective stress mitigation and ROS control (Fujita and Hasanuzzaman 2022). SOD

converts superoxide radicals into H_2O_2, which is subsequently detoxified by CAT and APX, whereas PPO contributes to phenolic oxidation and stress defense. The coordinated regulation of these enzymes in treated plants demonstrates improved antioxidant balance and ROS homeostasis (Mondal et al. 2023). The strong positive correlations among antioxidant enzymes, osmolyte accumulation, and physiological performance further support the existence of an integrated protective network activated by nanoparticle and ANE application.

Expression analysis of stress-responsive genes provided additional evidence for the protective effects of MNS, nano-Fe, and *A. nodosum* extract under saline conditions. Salinity stress markedly upregulated the expression of *ZmDREB2A*, *ZmHSP70*, *ZmP5CS*, *ZmCAT1*, and *ZmNHX1*, indicating activation of osmotic adjustment, antioxidant defense, ion transport regulation, and stress signaling pathways. The enhanced expression of *ZmDREB2A* suggests activation of transcriptional regulation associated with abiotic stress tolerance (Filyushin et al. 2022), while increased *ZmHSP70* expression reflects protection of cellular proteins and maintenance of protein folding under stress conditions (Zhao et al. 2021). Upregulation of *ZmP5CS* corresponded with increased proline accumulation and improved osmotic adjustment (Zhao et al. 2021), whereas enhanced *ZmCAT1* expression confirmed activation of antioxidant detoxification pathways (Pan et al. 2024). Increased expression of *ZmNHX1* further indicated improved vacuolar sequestration of Na^+ and maintenance of ionic homeostasis in treated plants (Liu et al. 2025). The combined application of MNS + Nano-Fe + ANE produced the most coordinated expression patterns of stress-responsive genes, demonstrating the effectiveness of integrated nano-enabled biostimulant treatments in improving molecular adaptation and stress resilience in maize plants.

The correlation heatmap provided additional mechanistic evidence for the integrated role of nanoparticles and biostimulants in salinity tolerance. Positive correlations among chlorophyll pigments, gas exchange traits, nutrient accumulation, soluble proteins, antioxidant enzymes, and stress-responsive gene expression indicated coordinated enhancement of photosynthetic efficiency, antioxidant defense, and metabolic activity. In contrast, strong negative correlations between oxidative markers (MDA and H_2O_2) and physiological traits demonstrated the inhibitory effects of oxidative stress on plant performance. These relationships confirm that alleviation of oxidative damage and maintenance of ion homeostasis are central mechanisms involved in sustaining physiological and biochemical functionality under saline conditions. The findings

demonstrate that the synergistic interaction among mesoporous nano-silica, nano-iron, and *A. nodosum* extract effectively improved salinity tolerance in maize plants through integrated regulation of physiological, biochemical, antioxidant, nutritional, and molecular defense mechanisms.

Conclusion

The present study demonstrated that salinity stress severely impaired maize growth and physiological performance through the induction of oxidative stress, disruption of nutrient homeostasis, inhibition of photosynthetic activity, and alteration of metabolic stability. Increasing salinity levels significantly reduced biomass accumulation, chlorophyll pigments, gas exchange characteristics, and macro- and micronutrient uptake, while simultaneously increasing sodium accumulation, lipid peroxidation, hydrogen peroxide production, and antioxidant enzyme activities. These physiological, biochemical, and nutritional disturbances collectively contributed to growth suppression and reduced stress tolerance under saline conditions.

In contrast, the application of mesoporous nano-silica (MNS), nano-iron (Nano-Fe), and *A. nodosum* extract (ANE), particularly when applied in combined formulations, effectively alleviated the detrimental effects of salinity stress. The integrated treatment of MNS + Nano-Fe + ANE produced the greatest improvements in plant growth, biomass production, photosynthetic efficiency, osmotic adjustment, antioxidant defense capacity, nutrient acquisition, ion homeostasis, and metabolic stability. In addition, the combined treatment enhanced the expression of stress-responsive genes associated with antioxidant defense, osmotic regulation, and ion transport, indicating improved molecular adaptation under saline conditions. These beneficial effects were closely associated with reduced oxidative damage, enhanced ROS detoxification, improved nutrient balance, preservation of chloroplast functionality, stabilization of cellular membranes, and maintenance of physiological activity.

The synergistic interaction among silicon-mediated structural protection, iron-driven metabolic activation, and ANE-induced physiological and biochemical stimulation highlights the strong potential of integrated nano-enabled biostimulant strategies for improving maize resilience under saline environments. Mesoporous nano-silica contributed to membrane stabilization and ionic regulation, nano-iron improved chlorophyll biosynthesis and metabolic activity, while *A. nodosum* extract enhanced antioxidant defense, osmotic adjustment, and stress-responsive signaling

pathways. The coordinated regulation of these protective mechanisms enabled maize plants to better tolerate salinity-induced stress conditions.

The findings indicate that the combined application of mesoporous nano-silica, nano-iron, and *A. nodosum* extract represents an effective, sustainable, and environmentally friendly strategy for enhancing salinity tolerance, maintaining physiological and metabolic performance, and improving maize productivity under salt-affected conditions. These nano-enabled biostimulant approaches may provide promising opportunities for sustainable crop management and climate-resilient agricultural systems in saline and arid regions.

Acknowledgements

This research has been funded by Scientific Research Deanship at University of Hail – Saudi Arabia through project number RG-25 087.

Data availability

The raw data supporting the conclusions of this article will be made available by the authors, without undue restriction, upon reasonable request to the corresponding author.

Conflicts of interest/Competing interests

The authors declare that they have no known competing financial interests or personal relationships that could have appeared to influence the work reported in this paper.

Availability of data and material

All data generated or analyzed during this study will be made available by the corresponding author upon reasonable request.

Funded

This research has been funded by Scientific Research Deanship at University of Hail – Saudi Arabia through project number RG-25 087.

Author Contribution

Data curation: Wasimah B. Al-Shammari, Haya Altamimi, & Dalal Alenizi; Formal Analysis:Hanan Khalaf Anazi, Habibah A Almalawi, & Kholoud Alshammery; Funding

Acquisition:Wasimah B. Al-Shammari; Project Administration: Mona H. Soliman, Wasimah B. Al-Shammari 1, Dalal Alenizi; Resources: Haya Altamimi, Kholoud Alshammery, Jawaher Alrashdi,. Supervision: Mona H. Soliman, & Wasimah AlShammari; Writing—original draft, Mona H. Soliman, Habibah A Almalawi,Hanan Khalaf Anazi, Wasimah AlShammari, & Dalal Alenizi. All authors read and approved the final manuscript.

References

Abdulvawhab MH, Amiri J, Jabbarzadeh Z, Ansari A (2026) Nano-iron modulates salt stress responses in Lycium barbarum via enhanced nutrient uptake, antioxidant defense, and phenolic metabolism. BMC Plant Biology

Aebi H (1984) [13] Catalase in vitro. In: Methods in enzymology, vol 105. Elsevier, pp 121-126

Ahmad R, Hussain S, Anjum MA, Khalid MF, Saqib M, Zakir I, Hassan A, Fahad S, Ahmad S (2019) Oxidative stress and antioxidant defense mechanisms in plants under salt stress. In: Plant abiotic stress tolerance: Agronomic, molecular and biotechnological approaches. Springer, pp 191-205

Al-Shammari W, Alshammery K, Lotfi S, Altamimi H, Alshammari A, Al-Harbi NA, Rashed AA, Al-Shalawi M, Moustapha ME, Rashwan E (2025) Wheat salinity tolerance is enhanced by application of Bacillus megaterium or arbuscular mycorrhizal fungi via improving physio-biochemical and anatomical characteristics. BMC plant biology 25 (1):835

Al-Shammari WB, Al-Huquil AA, Alshammery K, Lotfi S, Altamimi H, Alshammari A, Al-Harbi NA, Rashed AA, Abdelaal K (2024) Alleviation of drought stress damages by melatonin and Bacillus thuringiensis associated with adjusting photosynthetic efficiency, antioxidative system, and anatomical structure of Glycine max (L.). Heliyon 10 (14)

Alam P, Arshad M, Al-Kheraif AA, Azzam MA, Al Balawi T (2022) Silicon nanoparticle-induced regulation of carbohydrate metabolism, photosynthesis, and ROS homeostasis in Solanum lycopersicum subjected to salinity stress. ACS omega 7 (36):31834-31844

Ali M, Afzal S, Parveen A, Kamran M, Javed MR, Abbasi GH, Malik Z, Riaz M, Ahmad S, Chattha MS (2021) Silicon mediated improvement in the growth and ion homeostasis by decreasing Na+ uptake in maize (Zea mays L.) cultivars exposed to salinity stress. Plant Physiology and Biochemistry 158:208-218

Alshammari WB, Alshammery K, Lotfi S, Altamimi H, Alshammari A, Al-Harbi NA, Jakovljević D, Alharbi MH, Moustapha ME, Abd El-Moneim D (2024) Improvement of morphophysiological and anatomical attributes of plants under abiotic stress conditions using plant growth-promoting bacteria and safety treatments. PeerJ 12:e17286

Aqaei P, Weria W, Marjan D, Javad R, and Struik PC (2020) Response of maize (Zea mays L.) to potassium nano-silica application under drought stress. Journal of Plant Nutrition 43 (9):1205-1216. doi:10.1080/01904167.2020.1727508

Awais M, Rafiq M, Shabbir R, Aslam M (2023) Salinity stress effects on nutrient uptake in plants and its influence on plant growth efficiency. Trends Anim Plant Sci 1:64-72

Balasubramaniam T, Shen G, Esmaeili N, Zhang H (2023) Plants' response mechanisms to salinity stress. Plants 12 (12):2253

Bates LS, Waldren R, Teare I (1973) Rapid determination of free proline for water-stress studies. Plant and soil 39:205-207

Bhardwaj A, Bhatt U, Parihar S, Soni V (2025) Beyond osmoprotection: the expanding roles of proline in plant signalling and development. Biologia Futura:1-20

Biancarosa I, Belghit I, Bruckner CG, Liland NS, Waagbø R, Amlund H, Heesch S, Lock EJ (2018) Chemical characterization of 21 species of marine macroalgae common in Norwegian waters: benefits of and limitations to their potential use in food and feed. Journal of the Science of Food and Agriculture 98 (5):2035-2042

Bradford MM (1976) A rapid and sensitive method for the quantitation of microgram quantities of protein utilizing the principle of protein-dye binding. Analytical biochemistry 72 (1-2):248-254

Bremner J (1965) Total nitrogen. Methods of soil analysis: part 2 chemical and microbiological properties 9:1149-1178

Bustin SA, Benes V, Garson JA, Hellemans J, Huggett J, Kubista M, Mueller R, Nolan T, Pfaffl MW, Shipley GL (2009) The MIQE Guidelines: M inimum I nformation for Publication of Q uantitative Real-Time PCR E xperiments. Oxford University Press,

Dang J, Ma L, Nai G, Sun P, Zhang J, Li Z, Liu Y, Song X, Feng L, Li S (2026) Physiological, Biochemical and Transcriptomic Mechanisms Underlying the Mitigation of Salt Stress in Cabernet Sauvignon Grapevine Seedlings by Foliar Application of a Seaweed-Based Biostimulant (Jinmei Extract). Agriculture 16 (6):636

Darakeh SASS, Weisany W, Tahir NA-R, Schenk PM (2022) Physiological and biochemical responses of black cumin to vermicompost and plant biostimulants: Arbuscular mycorrhizal and plant growth-promoting rhizobacteria. Industrial Crops and Products 188:115557. doi:https://doi.org/10.1016/j.indcrop.2022.115557

Dell'Aversana E, Cirillo V, Van Oosten MJ, Di Stasio E, Saiano K, Woodrow P, Ciarmiello LF, Maggio A, Carillo P (2021) Ascophyllum nodosum based extracts counteract salinity stress in tomato by remodeling leaf nitrogen metabolism. Plants 10 (6):1044

El-Desouky HS, Islam KR, Bergefurd B, Gao G, Harker T, Abd-El-Dayem H, Ismail F, Mady M, Zewail RM (2021) Nano iron fertilization significantly increases tomato yield by increasing plants' vegetable growth and photosynthetic efficiency. Journal of Plant Nutrition 44 (11):1649-1663

Farajollahi Z, Eisvand HR, Nazarian-Firouzabadi F, Nasrollahi AH (2023) Nano-Fe nutrition improves soybean physiological characteristics, yield, root features and water productivity in different planting dates under drought stress conditions. Industrial Crops and Products 198:116698

Filyushin MA, Kochieva EZ, Shchennikova AV (2022) ZmDREB2. 9 gene in maize (Zea mays L.): genome-wide identification, characterization, expression, and stress response. Plants 11 (22):3060

Fujita M, Hasanuzzaman M (2022) Approaches to enhancing antioxidant defense in plants. vol 11. MDPI,

Ghawana S, Paul A, Kumar H, Kumar A, Singh H, Bhardwaj PK, Rani A, Singh RS, Raizada J, Singh K (2011) An RNA isolation system for plant tissues rich in secondary metabolites. BMC research notes 4 (1):85

Ghosh PK, Ghosh C (2023) Current Avenues in Nutraceuticals and Pharmaceuticals from Algae. Current Nutraceuticals 4 (1):e180523217061

Ghouri F, Sarwar S, Sun L, Riaz M, Haider FU, Ashraf H, Lai M, Imran M, Liu J, Ali S (2024) Silicon and iron nanoparticles protect rice against lead (Pb) stress by improving oxidative tolerance and minimizing Pb uptake. Scientific Reports 14 (1):5986

Giannopolitis CN, Ries SK (1977) Superoxide Dismutases: I. Occurrence in Higher Plants 1 2. Plant Physiology 59 (2):309-314. doi:10.1104/pp.59.2.309

Goñi O, Quille P, O'Connell S (2018) Ascophyllum nodosum extract biostimulants and their role in enhancing tolerance to drought stress in tomato plants. Plant Physiology and Biochemistry 126:63-73

Heath RL, Packer L (1968) Photoperoxidation in isolated chloroplasts: II. Role of electron transfer. Archives of biochemistry and biophysics 125 (3):850-857

Hussain T, Li J, Feng X, Asrar H, Gul B, Liu X (2021) Salinity induced alterations in photosynthetic and oxidative regulation are ameliorated as a function of salt secretion. Journal of plant research 134 (4):779-796

Islam M, Islam M, Hasan M, Hafeez A, Chowdhury M, Pramanik M, Iqbal M, Erman M, Barutcular C, Konuşkan Ö (2024) Salinity stress in maize: consequences, tolerance mechanisms, and management strategies. OBM Genetics 8 (2)

Johnson R, Joel JM, Puthur JT (2024) Biostimulants: The futuristic sustainable approach for alleviating crop productivity and abiotic stress tolerance. Journal of Plant Growth Regulation 43 (3):659-674

Jones J, Jr (1991) Kjeldahl method for nitrogen determination.

Khan M, Panda S (2008) Alterations in root lipid peroxidation and antioxidative responses in two rice cultivars under NaCl-salinity stress. Acta Physiologiae Plantarum 30 (1):81-89

Koleva L, Umar A, Yasin NA, Shah AA, Siddiqui MH, Alamri S, Riaz L, Raza A, Javed T, Shabbir Z (2022) Iron oxide and silicon nanoparticles modulate mineral nutrient homeostasis and metabolism in cadmium-stressed Phaseolus vulgaris. Frontiers in Plant Science 13:806781

Kumari S, Sehrawat KD, Phogat D, Sehrawat AR, Chaudhary R, Sushkova SN, Voloshina MS, Rajput VD, Shmaraeva AN, Marc RA (2023) Ascophyllum nodosum (L.) Le Jolis, a pivotal biostimulant toward sustainable agriculture: A comprehensive review. Agriculture 13 (6):1179

Li X, Yang S, Zhang J, Wan S (2026) Photo-Oxidative Stress in Plants: ROS Signaling, Damage Propagation, and Systems-Level Resilience. Antioxidants 15 (3):371

Liang Y, Liu H, Fu Y, Li P, Li S, Gao Y (2023) Regulatory effects of silicon nanoparticles on the growth and photosynthesis of cotton seedlings under salt and low-temperature dual stress. BMC Plant Biology 23 (1):504

Lichtenthaler HK, Wellburn AR (1983) Determinations of total carotenoids and chlorophylls a and b of leaf extracts in different solvents. Portland Press Ltd.,

Liu HS, Liu Q, Hepworth SR, Li PQ, Huang J, Zhang RX, Ma CM, Gao TG, Ma HP, Ke J (2025) ZxNHX1 from a xerophyte outperforms AtNHX1 in sequestering Na+ into vacuoles to enhance plant stress resistance and yield. Plant Biotechnology Journal 23 (9):3497-3509
Livak KJ, Schmittgen TD (2001) Analysis of relative gene expression data using real-time quantitative PCR and the 2− ΔΔCT method. methods 25 (4):402-408
Mæhre HK, Malde MK, Eilertsen KE, Elvevoll EO (2014) Characterization of protein, lipid and mineral contents in common Norwegian seaweeds and evaluation of their potential as food and feed. Journal of the Science of Food and Agriculture 94 (15):3281-3290
Mayer AM, Harel E (1979) Polyphenol oxidases in plants. Phytochemistry 18 (2):193-215
Minkov P, Gechev TS, Kanojia A (2026) Terrestrial Plant-and Algal-Derived Biostimulants as Modulators of ROS and Hormone Networks in Crop Abiotic Stress Resilience. Plants 15 (7):992
Mondal S, Burgert S, Asch J, Rahaman EHMS, Asch F (2023) Salinity effects on the activities of ROS scavenging enzymes in leaves of two sweet potato clones. Journal of Agronomy and Crop Science 209 (6):841-853
Murphy J, Riley JP (1962) A modified single solution method for the determination of phosphate in natural waters. Analytica chimica acta 27:31-36
Nakano Y, Asada K (1981) Hydrogen peroxide is scavenged by ascorbate-specific peroxidase in spinach chloroplasts. Plant and cell physiology 22 (5):867-880
Olaetxea M, Garnica M, Erro J, Sanz J, Monreal G, Zamarreño AM, García-Mina JM (2024) The plant growth-promoting effect of an Ascophyllum nodosum (L.) extract derives from the interaction of its components and involves salicylic-, auxin-and cytokinin-signaling pathways. Chemical and Biological Technologies in Agriculture 11 (1):190
Pan Y, Han T, Xiang Y, Wang C, Zhang A (2024) The transcription factor ZmNAC84 increases maize salt tolerance by regulating ZmCAT1 expression. The Crop Journal 12 (5):1344-1356
Pratt PF, Chapman HD (1961) Gains and losses of mineral elements in an irrigated soil during a 20-year lysimeter investigation.
Rao MJ, Duan M, Zhou C, Jiao J, Cheng P, Yang L, Wei W, Shen Q, Ji P, Yang Y (2025) Antioxidant defense system in plants: reactive oxygen species production, signaling, and scavenging during abiotic stress-induced oxidative damage. Horticulturae 11 (5):477
Repke RA, Silva DMR, Dos Santos JCC, de Almeida Silva M (2022) Increased soybean tolerance to high-temperature through biostimulant based on Ascophyllum nodosum (L.) seaweed extract. Journal of Applied Phycology 34 (6):3205-3218
Sardans J, Peñuelas J (2021) Potassium control of plant functions: Ecological and agricultural implications. Plants 10 (2):419
Sepehrzadegan Z, Alizadeh O (2021) Investigation of the growth bacteria and Nano iron on the chlorophyll and some nutrients triticale. Rev Agrogeoambiental 13 (10.18406)
Shahid MA, Sarkhosh A, Khan N, Balal RM, Ali S, Rossi L, Gómez C, Mattson N, Nasim W, Garcia-Sanchez F (2020) Insights into the physiological and biochemical impacts of salt stress on plant growth and development. Agronomy 10 (7):938
Shukla PS, Mantin EG, Adil M, Bajpai S, Critchley AT, Prithiviraj B (2019) Ascophyllum nodosum-based biostimulants: Sustainable applications in agriculture for the stimulation of plant growth, stress tolerance, and disease management. Frontiers in plant science 10:462648

Singh M, Kumar J, Singh S, Singh VP, Prasad SM (2015) Roles of osmoprotectants in improving salinity and drought tolerance in plants: a review. Reviews in environmental science and bio/technology 14 (3):407-426
Soares C, Pereira R, Fidalgo F (2018) Metal-based nanomaterials and oxidative stress in plants: current aspects and overview. In: Phytotoxicity of nanoparticles. Springer, pp 197-227
Tee JK, Ong CN, Bay BH, Ho HK, Leong DT (2016) Oxidative stress by inorganic nanoparticles. Wiley Interdisciplinary Reviews: Nanomedicine and Nanobiotechnology 8 (3):414-438
US E (1996) Method 3052: microwave assisted and digestion of siliceous and organically based matrices. Washington, DC
Velikova V, Yordanov I, Edreva A (2000) Oxidative stress and some antioxidant systems in acid rain-treated bean plants: protective role of exogenous polyamines. Plant science 151 (1):59-66
Wang D, Hou L, Zhang L, Liu P (2021) The mechanisms of silicon on maintaining water balance under water deficit stress. Physiologia Plantarum 173 (3):1253-1262
Weisany W, Khosropour E (2023) Chapter 8 - Engineered nanomaterials in crop plants drought stress management. In: Husen A (ed) Engineered Nanomaterials for Sustainable Agricultural Production, Soil Improvement and Stress Management. Academic Press, pp 183-204. doi:https://doi.org/10.1016/B978-0-323-91933-3.00005-2
Weisany W, Razmi J, Eshaghabadi AH, Pashang D (2024) Silicon Nanoparticles (SiNP): A Novel and Sustainable Strategy for Mitigating Environmental Stresses in Plants. Journal of Soil Science and Plant Nutrition 24 (2):2167-2191. doi:10.1007/s42729-024-01790-1
Weisany W, Razmi J, Pashang D (2023) Improving seed germination and physiological characteristics of maize seedlings under osmotic stress through potassium nano-silicate treatment. Frontiers in Plant Science 14:1274396
Yan G, Zhao S, Dong J, Qiu H, Li B, Cao L, Yuan T, Zhu X, Mao S, Wang P (2025) Silicon enhances root potassium retention in cucumber under salt stress through promoting sodium exclusion and antioxidant capacity. Plant Physiology and Biochemistry 227:110156
Zhao Y, Du H, Wang Y, Wang H, Yang S, Li C, Chen N, Yang H, Zhang Y, Zhu Y (2021) The calcium-dependent protein kinase ZmCDPK7 functions in heat-stress tolerance in maize. Journal of Integrative Plant Biology 63 (3):510-527

Table 1. Physicochemical properties of the experimental soil

Sand	Silt	Clay	pH	EC	OC	N	P	K	Fe	Cu	Zn	Si
(%)				(dS m^{-1})	(%)	(%)	(mg kg^{-1})					
45	20	35	7.31	1.23	1.28	0.92	95.2	481.1	6.75	2.6	1.85	18.4

EC = Electrical conductivity; OC = Organic carbon; N = Nitrogen; P = Phosphorus; K = Potassium; Fe = Iron; Cu = Copper; Zn = Zinc; Si = Silicon; pH = Potential of hydrogen.

Table 2. Proximate composition and mineral content of *Ascophyllum nodosum*.

Species	Crude Lipids	T. protein	Crude fiber	Carbohydrates	Moisture	Ashes content	N	P	K	Mg	Ca	Na
	(%)						(g kg^{-1} DW)					
Ascophyllum nodosum	2.70	7.40	43.60	16.30	10.70	19.30	11.8	1.30	38.7	15.4	10.6	42.3

Table 3. Effects of salinity stress, mesoporous nano-silica (MNS), nano-iron (Nano-Fe), and *Ascophyllum nodosum* extract (ANE) on morphological traits of safflower plants

Salinity (mM NaCl)	Treatment	Plant height (cm)	Fresh weight (g plant^{-1})	Dry weight (g plant^{-1})	Number of leaves (plant^{-1})
0	Control	69.25 ± 1.95 h	46.85 ± 2.15 h	12.80 ± 0.58 i	29.40 ± 1.28 i
	MNS	73.62 ± 2.30 e	51.10 ± 2.42 e	14.25 ± 0.66 f	32.75 ± 1.54 f
	Nano-Fe	75.85 ± 2.55 d	53.45 ± 2.78 d	15.10 ± 0.72 e	34.62 ± 1.62 e
	ANE	72.42 ± 2.18 f	49.95 ± 2.36 f	13.91 ± 0.64 g	31.79 ± 1.46 g

Salinity (mM NaCl)	Treatment	Plant height (cm)	Fresh weight (g plant^{-1})	Dry weight (g plant^{-1})	Number of leaves (plant^{-1})
	MNS + Nano-Fe	78.95 ± 2.72 b	56.82 ± 2.95 b	16.25 ± 0.80 b	36.45 ± 1.75 b
	MNS + ANE	76.20 ± 2.48 d	54.60 ± 2.70 c	15.45 ± 0.76 d	35.12 ± 1.68 d
	Nano-Fe + ANE	77.49 ± 2.60 c	55.92 ± 2.84 bc	15.82 ± 0.79 c	35.85 ± 1.72 c
	MNS + Nano-Fe + ANE	81.30 ± 2.88 a	59.75 ± 3.10 a	17.45 ± 0.86 a	38.59 ± 1.90 a
75	Control	54.40 ± 1.72 n	33.15 ± 1.88 n	8.95 ± 0.48 n	22.09 ± 1.12 n
	MNS	59.26 ± 1.96 l	37.80 ± 2.05 l	10.45 ± 0.54 l	25.85 ± 1.26 l
	Nano-Fe	61.75 ± 2.05 k	40.21 ± 2.18 k	11.30 ± 0.60 k	27.45 ± 1.34 k
	ANE	58.14 ± 1.88 m	36.60 ± 1.96 m	10.05 ± 0.52 m	24.95 ± 1.22 m
	MNS + Nano-Fe	65.31 ± 2.18 i	43.85 ± 2.34 i	12.40 ± 0.66 j	30.19 ± 1.48 j
	MNS + ANE	63.25 ± 2.12 j	41.95 ± 2.26 j	11.95 ± 0.62 j	28.85 ± 1.40 j
	Nano-Fe + ANE	64.85 ± 2.16 i	42.75 ± 2.30 ij	12.15 ± 0.64 j	29.40 ± 1.45 i
	MNS + Nano-Fe + ANE	68.40 ± 2.35 h	46.55 ± 2.48 h	13.55 ± 0.70 h	32.09 ± 1.55 h
150	Control	39.16 ± 1.34 s	21.45 ± 1.36 s	5.35 ± 0.30 s	15.61 ± 0.88 s
	MNS	45.14 ± 1.52 q	26.74 ± 1.58 q	6.95 ± 0.38 q	18.85 ± 0.96 q
	Nano-Fe	48.25 ± 1.66 p	28.95 ± 1.72 p	7.80 ± 0.44 p	20.40 ± 1.05 p
	ANE	44.19 ± 1.46 r	25.42 ± 1.50 r	6.55 ± 0.36 r	17.95 ± 0.92 r

Salinity (mM NaCl)	Treatment	Plant height (cm)	Fresh weight (g plant^{-1})	Dry weight (g plant^{-1})	Number of leaves (plant^{-1})
	MNS + Nano-Fe	53.75 ± 1.84 o	33.25 ± 1.95 n	9.35 ± 0.51 n	23.79 ± 1.18 n
	MNS + ANE	50.95 ± 1.76 p	31.45 ± 1.82 o	8.71 ± 0.47 o	22.45 ± 1.10 o
	Nano-Fe + ANE	52.11 ± 1.80 o	32.15 ± 1.88 no	8.95 ± 0.48 n	23.11 ± 1.15 no
	MNS + Nano-Fe + ANE	57.85 ± 1.98 m	36.90 ± 2.05 m	10.75 ± 0.58 l	26.95 ± 1.30 l

Values are presented as mean ± SE of four replicates. Different letters within each column indicate significant differences according to the LSD test at $p \leq 0.05$.

Table 4. Effects of salinity stress, mesoporous nano-silica (MNS), nano-iron (Nano-Fe), and *Ascophyllum nodosum* extract (ANE) on photosynthetic pigments of safflower plants

Salinity (mM NaCl)	Treatment	Chlorophyll a	Chlorophyll b	Total chlorophyll	Carotenoids
		(mg g^{-1} FW)			
0	Control	1.92 ± 0.08 h	0.75 ± 0.032 j	2.67 ± 0.12 h	0.60 ± 0.028 i
	MNS	2.08 ± 0.10 e	0.82 ± 0.038 f	2.92 ± 0.14 e	0.66 ± 0.031 f
	Nano-Fe	2.15 ± 0.11 d	0.86 ± 0.042 e	3.01 ± 0.15 d	0.69 ± 0.034 e
	ANE	2.02 ± 0.09 g	0.81 ± 0.036 h	2.82 ± 0.13 g	0.64 ± 0.030 g
	MNS + Nano-Fe	2.28 ± 0.12 b	0.92 ± 0.045 b	3.20 ± 0.16 b	0.74 ± 0.038 b
	MNS + ANE	2.19 ± 0.11 c	0.88 ± 0.043 d	3.06 ± 0.15 c	0.71 ± 0.035 d
	Nano-Fe + ANE	2.22 ± 0.11 bc	0.91 ± 0.044 c	3.12 ± 0.16 bc	0.72 ± 0.036 c
	MNS + Nano-Fe + ANE	2.40 ± 0.13 a	0.98 ± 0.048 a	3.38 ± 0.18 a	0.79 ± 0.040 a
75	Control	1.42 ± 0.07 p	0.58 ± 0.026 p	2.01 ± 0.10 p	0.46 ± 0.021 p
	MNS	1.66 ± 0.08 l	0.67 ± 0.031 m	2.32 ± 0.12 l	0.53 ± 0.024 l
	Nano-Fe	1.75 ± 0.09 j	0.71 ± 0.034 l	2.46 ± 0.13 j	0.57 ± 0.027 j
	ANE	1.58 ± 0.08 m	0.64 ± 0.030 n	2.22 ± 0.11 m	0.51 ± 0.023 m
	MNS + Nano-Fe	1.92 ± 0.10 h	0.78 ± 0.037 i	2.72 ± 0.14 h	0.63 ± 0.030 h
	MNS + ANE	1.81 ± 0.09 i	0.74 ± 0.035 k	2.56 ± 0.13 i	0.60 ± 0.028 i
	Nano-Fe + ANE	1.86 ± 0.09 hi	0.76 ± 0.036 ij	2.62 ± 0.14 hi	0.61 ± 0.029 hi

Salinity (mM NaCl)	Treatment	Chlorophyll a	Chlorophyll b	Total chlorophyll	Carotenoids
		(mg g^{-1} FW)			
	MNS + Nano-Fe + ANE	2.02 ± 0.10 f	0.84 ± 0.040 ef	2.86 ± 0.15 f	0.67 ± 0.032 ef
150	Control	0.98 ± 0.05 s	0.41 ± 0.018 s	1.38 ± 0.07 s	0.31 ± 0.015 s
	MNS	1.28 ± 0.06 q	0.52 ± 0.023 q	1.80 ± 0.09 q	0.39 ± 0.018 q
	Nano-Fe	1.39 ± 0.07 p	0.58 ± 0.027 o	1.96 ± 0.10 p	0.45 ± 0.021 p
	ANE	1.22 ± 0.06 r	0.51 ± 0.022 r	1.71 ± 0.08 r	0.38 ± 0.017 r
	MNS + Nano-Fe	1.58 ± 0.08 m	0.66 ± 0.031 mn	2.24 ± 0.11 mn	0.52 ± 0.024 mn
	MNS + ANE	1.48 ± 0.07 o	0.62 ± 0.029 no	2.09 ± 0.10 o	0.49 ± 0.022 o
	Nano-Fe + ANE	1.52 ± 0.08 no	0.64 ± 0.030 n	2.16 ± 0.11 no	0.51 ± 0.023 no
	MNS + Nano-Fe + ANE	1.75 ± 0.09 k	0.72 ± 0.034 l	2.44 ± 0.13 k	0.58 ± 0.027 k

Values are expressed as mean ± SE of four replicates. Different letters within each column indicate significant differences according to the LSD test at $p \leq 0.05$.

Table 5. Effects of salinity stress, mesoporous nano-silica (MNS), nano-iron (Nano-Fe), and *Ascophyllum nodosum* extract (ANE) on gas exchange parameters of safflower plants

Salinity (mM NaCl)	Treatment	Net photosynthetic rate (µmol CO_2 m^{-2} s^{-1})	Stomatal conductance (mol H_2O m^{-2} s^{-1})	Transpiration rate (mmol H_2O m^{-2} s^{-1})	Intercellular CO_2 concentration (µmol mol^{-1})
0	Control	18.45 ± 0.92 j	0.42 ± 0.021 k	5.85 ± 0.30 l	268.39 ± 12.21 m
	MNS	20.80 ± 1.05 g	0.48 ± 0.024 g	6.35 ± 0.32 h	278.25 ± 13.20 i
	Nano-Fe	21.95 ± 1.10 e	0.52 ± 0.026 e	6.79 ± 0.35 f	286.91 ± 13.75 g
	ANE	20.45 ± 1.02 h	0.47 ± 0.023 h	6.38 ± 0.31 i	275.86 ± 13.05 j
	MNS + Nano-Fe	24.85 ± 1.25 b	0.58 ± 0.028 b	7.45 ± 0.38 b	298.59 ± 14.26 b
	MNS + ANE	23.62 ± 1.18 d	0.55 ± 0.027 d	7.09 ± 0.36 d	292.75 ± 14.01 d
	Nano-Fe + ANE	24.09 ± 1.22 c	0.56 ± 0.028 c	7.25 ± 0.37 c	295.22 ± 14.10 c
	MNS + Nano-Fe + ANE	27.45 ± 1.38 a	0.64 ± 0.032 a	8.08 ± 0.42 a	313.68 ± 14.95 a
	Control	12.85 ± 0.68 p	0.28 ± 0.014 q	4.05 ± 0.22 r	218.3 ± 10.45 s
75	MNS	15.62 ± 0.80 m	0.35 ± 0.018 m	4.75 ± 0.24 n	236.75 ± 11.09 o
	Nano-Fe	16.85 ± 0.86 k	0.39 ± 0.020 j	5.12 ± 0.26 k	245.20 ± 11.51 l
	ANE	15.11 ± 0.76 n	0.33 ± 0.017 o	4.55 ± 0.23 p	232.39 ± 10.91 q
	MNS + Nano-Fe	19.79 ± 0.98 i	0.47 ± 0.024 h	6.15 ± 0.31 j	274.09 ± 13.05 k

Salinity (mM NaCl)	Treatment	Net photosynthetic rate (µmol CO_2 m^{-2} s^{-1})	Stomatal conductance (mol H_2O m^{-2} s^{-1})	Transpiration rate (mmol H_2O m^{-2} s^{-1})	Intercellular CO_2 concentration (µmol mol^{-1})
	MNS + ANE	18.39 ± 0.92 j	0.43 ± 0.021 i	5.68 ± 0.28 m	265.59 ± 12.75 n
	Nano-Fe + ANE	19.12 ± 0.95 h	0.45 ± 0.022 f	5.08 ± 0.30 l	269.28 ± 12.92 m
	MNS + Nano-Fe + ANE	22.45 ± 1.12 f	0.54 ± 0.027 e	6.85 ± 0.35 e	287.45 ± 13.79 f
	Control	7.25 ± 0.40 x	0.16 ± 0.008 x	2.35 ± 0.12 x	162.79 ± 7.85 x
150	MNS	10.45 ± 0.55 u	0.21 ± 0.011 u	3.05 ± 0.16 u	188.65 ± 8.95 u
	Nano-Fe	11.60 ± 0.60 s	0.25 ± 0.013 s	3.3 ± 0.18 s	199.45 ± 9.42 s
	ANE	9.95 ± 0.52 v	0.19 ± 0.010 v	2.89 ± 0.15 v	182.20 ± 8.74 v
	MNS + Nano-Fe	14.95 ± 0.75 o	0.34 ± 0.017 n	4.82 ± 0.24 o	238.75 ± 11.20 p
	MNS + ANE	13.86 ± 0.70 q	0.29 ± 0.015 p	4.25 ± 0.22 q	225.60 ± 10.75 r
	Nano-Fe + ANE	14.19 ± 0.72 p	0.31 ± 0.016 r	4.45 ± 0.23 t	235.45 ± 10.91 t
	MNS + Nano-Fe + ANE	17.81 ± 0.90 l	0.39 ± 0.020 l	5.52 ± 0.28 g	258.79 ± 12.37 h

1 Values are expressed as mean ± SE of four replicates. Different letters within each column indicate
2 significant differences according to the LSD test at $p \leq 0.05$.

3

4

5

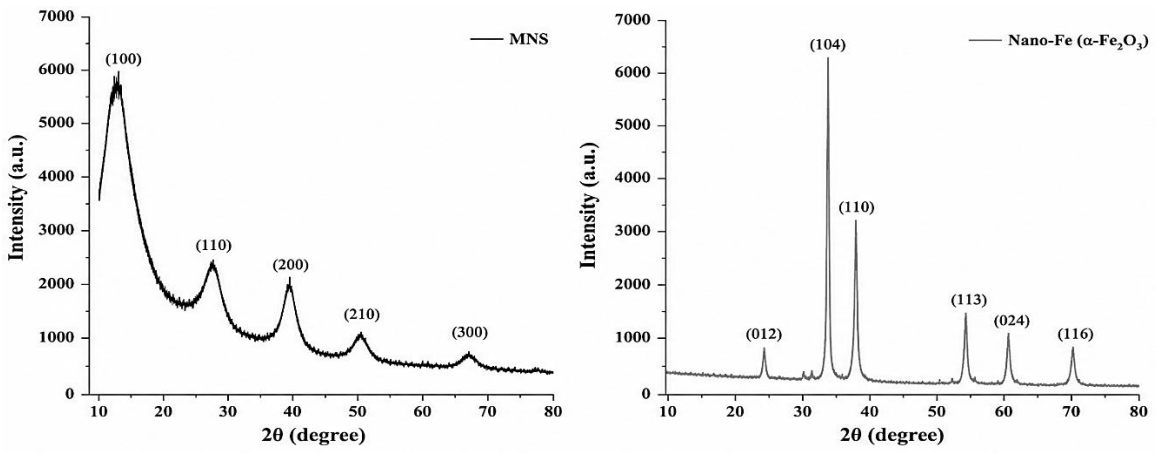
6

Table 6. Effects of salinity stress, mesoporous nano-silica (MNS), nano-iron (Nano-Fe), and *Ascophyllum nodosum* extract (ANE) on relative expression of stress-responsive genes in maize plants

Salinity (mM NaCl)	Treatment	ZmDREB2A	ZmHSP70	ZmP5CS	ZmCAT1	ZmNHX1
0	Control	1.01 ± 0.05 z	1.02 ± 0.04 y	1.03 ± 0.05 x	1.00 ± 0.05 w	1.02 ± 0.04 v
	MNS	1.31 ± 0.07 v	1.42 ± 0.08 t	1.29 ± 0.07 r	1.30 ± 0.06 p	1.42 ± 0.07 n
	Nano-Fe	1.51 ± 0.08 s	1.54 ± 0.09 q	1.45 ± 0.08 o	1.55 ± 0.07 m	1.63 ± 0.08 k
	ANE	1.39 ± 0.07 u	1.48 ± 0.08 s	1.34 ± 0.07 q	1.45 ± 0.07 o	1.49 ± 0.08 m
	MNS + Nano-Fe	1.95 ± 0.10 o	2.09 ± 0.12 m	1.88 ± 0.10 k	2.02 ± 0.10 i	2.15 ± 0.11 g
	MNS + ANE	1.82 ± 0.09 q	1.96 ± 0.10 o	1.76 ± 0.09 m	1.84 ± 0.09 k	2.01 ± 0.10 i
	Nano-Fe + ANE	1.89 ± 0.10 p	2.02 ± 0.11 n	1.82 ± 0.10 l	1.94 ± 0.10 j	2.08 ± 0.10 h
	MNS + Nano-Fe + ANE	2.35 ± 0.12 m	2.48 ± 0.14 k	2.22 ± 0.12 i	2.40 ± 0.12 g	2.62 ± 0.13 e

Salinity (mM NaCl)	Treatment	ZmDREB2A	ZmHSP70	ZmP5CS	ZmCAT1	ZmNHX1
	Control	3.84 ± 0.20 l	4.10 ± 0.22 j	4.25 ± 0.24 h	3.75 ± 0.20 f	4.44 ± 0.25 d
75	MNS	4.75 ± 0.26 j	5.11 ± 0.28 h	5.23 ± 0.30 f	4.62 ± 0.25 d	5.40 ± 0.30 b
	Nano-Fe	5.22 ± 0.30 h	5.55 ± 0.32 f	5.74 ± 0.34 d	5.18 ± 0.28 b	5.93 ± 0.35 z
	ANE	4.55 ± 0.25 k	4.84 ± 0.27 i	5.02 ± 0.28 g	4.42 ± 0.24 e	5.18 ± 0.29 c
	MNS + Nano-Fe	6.34 ± 0.36 d	6.92 ± 0.40 b	7.10 ± 0.42 z	6.21 ± 0.35 x	7.33 ± 0.44 v
	MNS + ANE	5.95 ± 0.34 f	6.45 ± 0.38 d	6.65 ± 0.39 b	5.85 ± 0.32 z	6.90 ± 0.40 x
	Nano-Fe + ANE	6.09 ± 0.35 e	6.70 ± 0.39 c	6.87 ± 0.41 a	6.0 ± 0.34 y	7.05 ± 0.41 w
	MNS + Nano-Fe + ANE	7.45 ± 0.42 b	8.11 ± 0.48 z	8.42 ± 0.50 v	7.35 ± 0.42 t	8.85 ± 0.52 r
	Control	8.65 ± 0.50 a	9.25 ± 0.55 v	9.75 ± 0.58 t	8.12 ± 0.48 r	10.45 ± 0.62 p
150	MNS	7.23 ± 0.42 c	7.80 ± 0.46 a	8.15 ± 0.48 w	7.05 ± 0.40 u	8.86 ± 0.52 s
	Nano-Fe	6.85 ± 0.40 d	7.37 ± 0.43 z	7.7 ± 0.46 x	6.75 ± 0.38 v	8.35 ± 0.50 t
	ANE	7.40 ± 0.43 b	7.95 ± 0.47 y	8.30 ± 0.49 u	7.15 ± 0.42 s	9.06 ± 0.54 q
	MNS + Nano-Fe	5.94 ± 0.34 g	6.41 ± 0.37 e	6.73 ± 0.39 c	5.88 ± 0.33 a	7.15 ± 0.41 u
	MNS + ANE	6.25 ± 0.36 f	6.75 ± 0.40 c	7.02 ± 0.41 y	6.10 ± 0.35 y	7.45 ± 0.43 y
	Nano-Fe + ANE	6.11 ± 0.35 g	6.03 ± 0.39 d	6.87 ± 0.40 z	5.9 ± 0.34 z	7.37 ± 0.42 z
	MNS + Nano-Fe + ANE	5.10 ± 0.28 i	5.55 ± 0.32 g	5.84 ± 0.34 e	5.02 ± 0.28 c	6.66 ± 0.36 a

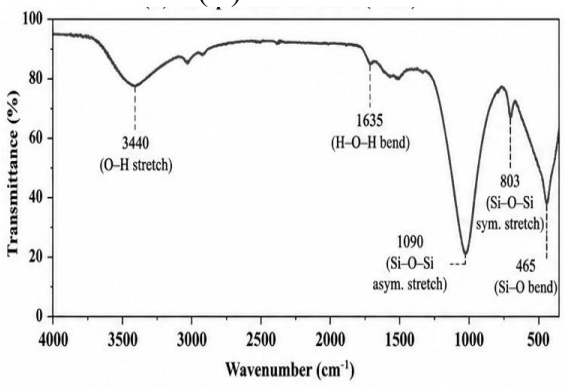
1 Values are expressed as mean ± SE of four replicates. Different letters within each column indicate
2 significant differences according to the LSD test at $p \leq 0.05$. Relative gene expression values were
3 calculated using the 2^-ΔΔCt method with actin used as the reference gene.


MNS
(100)
(110)
(200)
(210)
(300)
Intensity (a.u.)
2θ (degree)

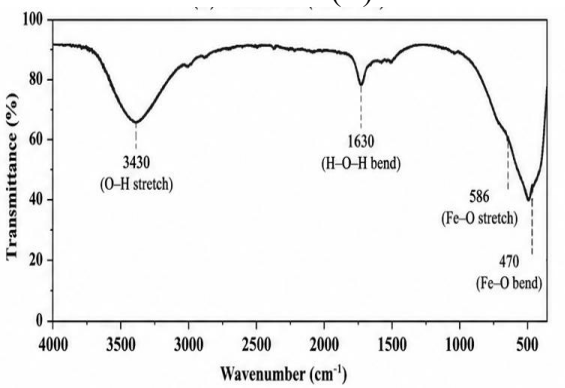
(A)

Nano-Fe (α-Fe2O3)
(104)
(110)
(012)
(113)
(024)
(116)
Intensity (a.u.)
2θ (degree)

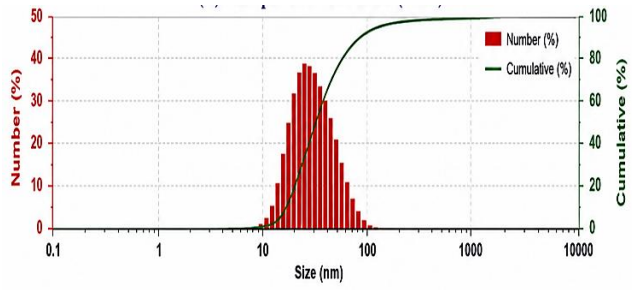
(B)

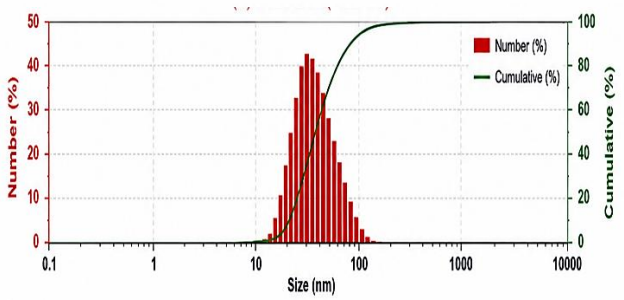

3440
(O–H stretch)
1635
(H–O–H bend)
1090
(Si–O–Si
asym. stretch)
803
(Si–O–Si
sym. stretch)
465
(Si–O bend)
Transmittance (%)
Wavenumber (cm-1)

(C)


3430
(O–H stretch)
1630
(H–O–H bend)
586
(Fe–O stretch)
470
(Fe–O bend)
Transmittance (%)
Wavenumber (cm-1)

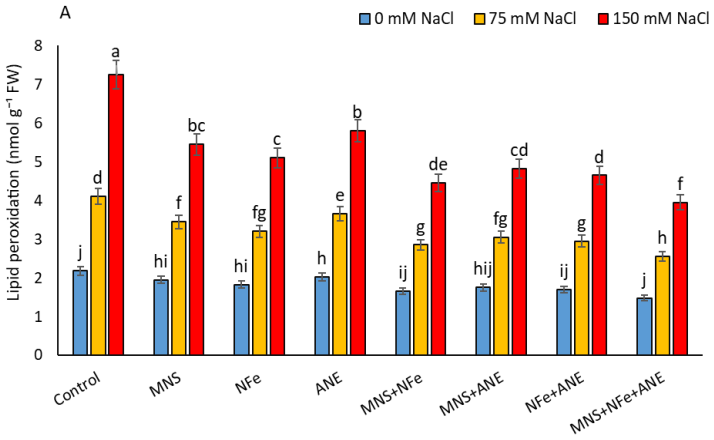
(D)

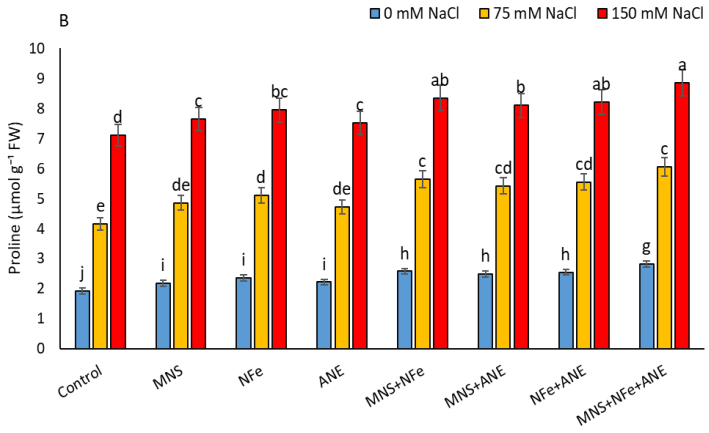

Number (%)
Cumulative (%)
Size (nm)


Number (%)
Cumulative (%)
Size (nm)

(E) (F)

Figure 1. Structural and physicochemical characterization of the synthesized nanoparticles. X-ray diffraction (XRD) patterns of (A) mesoporous nano-silica (MNS) and (B) nano-iron (Nano-Fe); Fourier transform infrared spectroscopy (FTIR) spectra of (C) MNS and (D) Nano-Fe showing characteristic functional groups and surface chemical bonding; and dynamic light scattering (DLS) analysis of (E) MNS and (F) Nano-Fe illustrating particle size distribution and cumulative particle percentage in aqueous suspension.





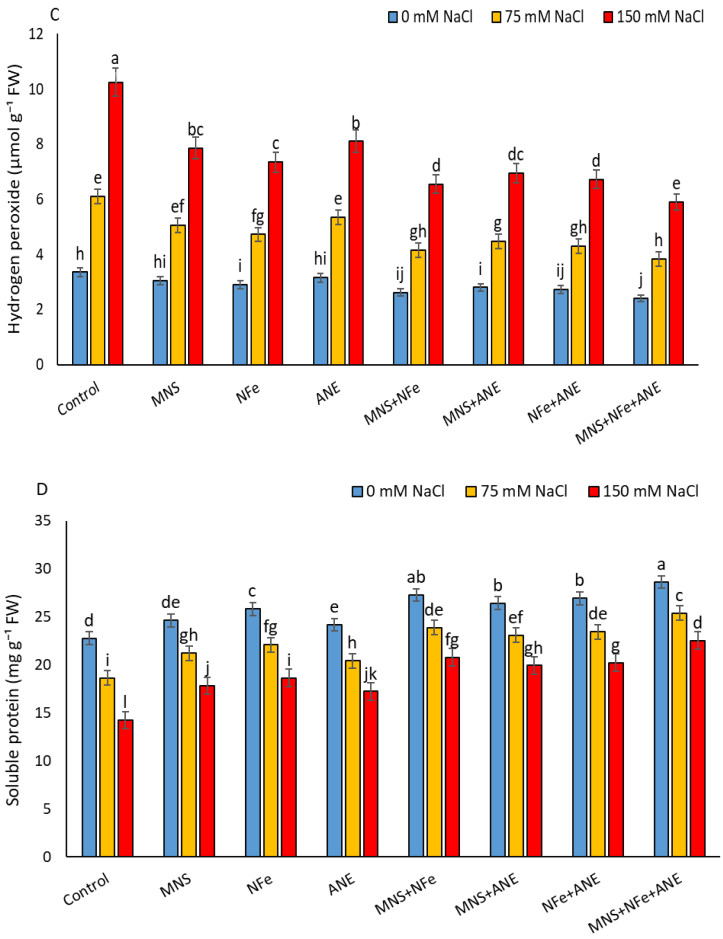
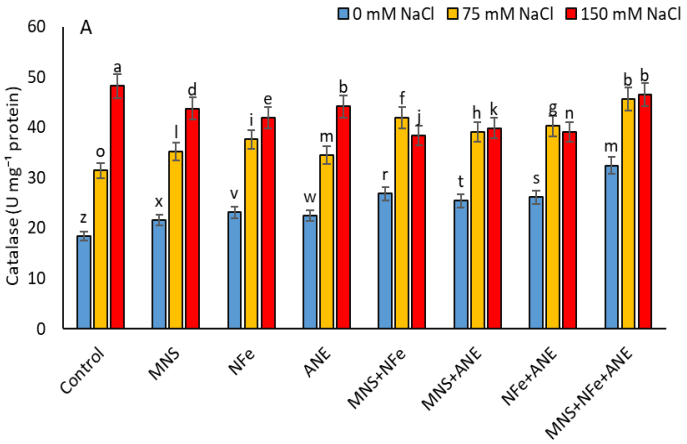


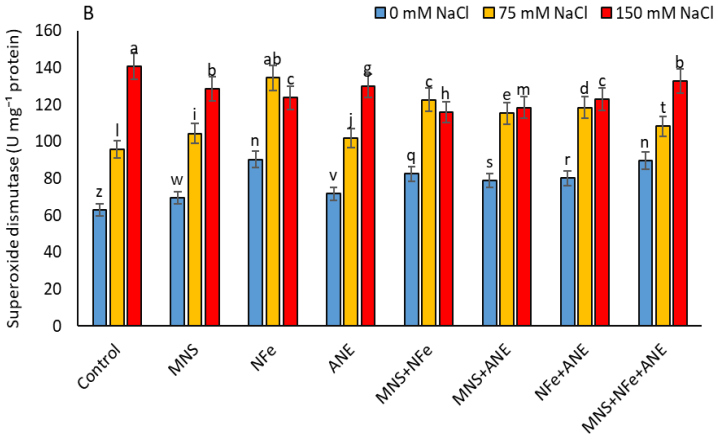
Figure 2. Effects of mesoporous nano-silica (MNS), nano-iron (NFe), and *Ascophyllum nodosum* extract (ANE), applied individually or in combination, on oxidative stress indicators and osmolyte accumulation in maize plants under different salinity levels (0, 75, and 150 mM NaCl). (A) lipid peroxidation (MDA content), (B) proline accumulation, (C) hydrogen peroxide content, and (D) soluble protein content. Values represent means ± SE of four replicates. Different letters above the bars indicate significant differences among treatments according to Duncan's multiple range test at $p \leq 0.05$.

1

2


A
0 mM NaCl
75 mM NaCl
150 mM NaCl
Catalase (U mg⁻¹ protein)
60
50
40
30
20
10
0
Control
MNS
NFe
ANE
MNS+NFe
MNS+ANE
NFe+ANE
MNS+NFe+ANE

3


B
0 mM NaCl
75 mM NaCl
150 mM NaCl
Superoxide dismutase (U mg⁻¹ protein)
160
140
120
100
80
60
40
20
0
Control
MNS
NFe
ANE
MNS+NFe
MNS+ANE
NFe+ANE
MNS+NFe+ANE

4

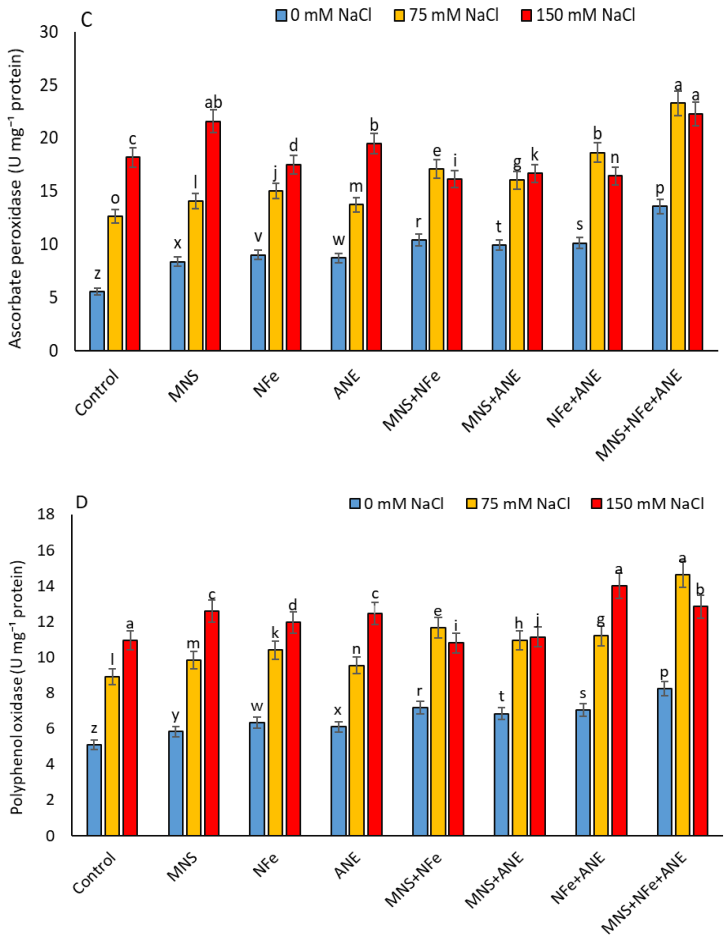
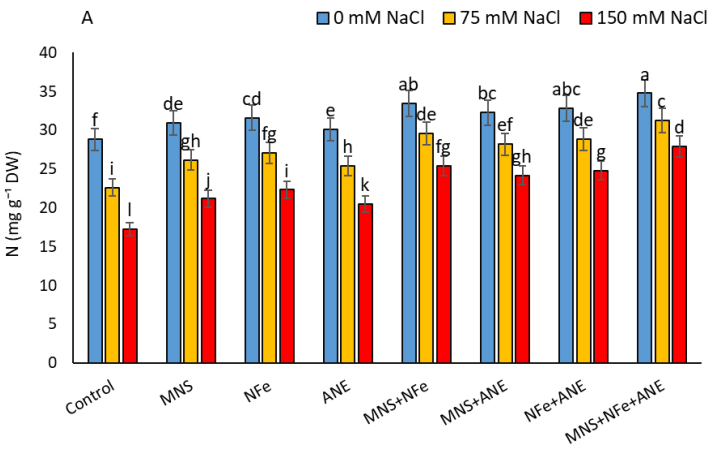
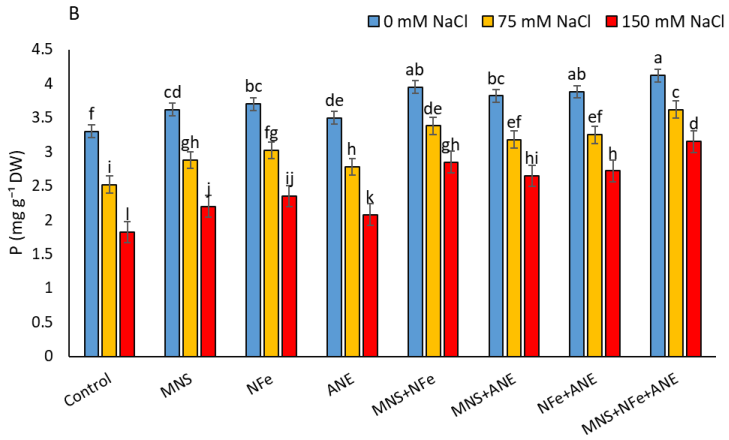


Figure 3. Effects of mesoporous nano-silica (MNS), nano-iron (NFe), and *Ascophyllum nodosum* extract (ANE), applied individually or in combination, on oxidative stress indicators and osmolyte accumulation in maize plants under different salinity levels (0, 75, and 150 mM NaCl). (A) catalase, (B) superoxide dismutase, (C) ascorbate peroxidase, and (D) polyphenol oxidase activity. Values represent means ± SE of four replicates. Different letters above the bars indicate significant differences among treatments according to Duncan's multiple range test at $p \leq 0.05$.


A
0 mM NaCl
75 mM NaCl
150 mM NaCl
N (mg g-1 DW)
40
35
30
25
20
15
10
5
0
f
i
l
de
gh
j
cd
fg
i
e
h
k
ab
de
fg
bc
ef
gh
abc
de
g
a
c
d
Control
MNS
NFe
ANE
MNS+NFe
MNS+ANE
NFe+ANE
MNS+NFe+ANE

1


B
0 mM NaCl
75 mM NaCl
150 mM NaCl
P (mg g-1 DW)
4.5
4
3.5
3
2.5
2
1.5
1
0.5
0
f
i
l
cd
gh
j
bc
fg
ij
de
h
k
ab
de
gh
bc
ef
hi
ab
ef
h
a
c
d
Control
MNS
NFe
ANE
MNS+NFe
MNS+ANE
NFe+ANE
MNS+NFe+ANE

2

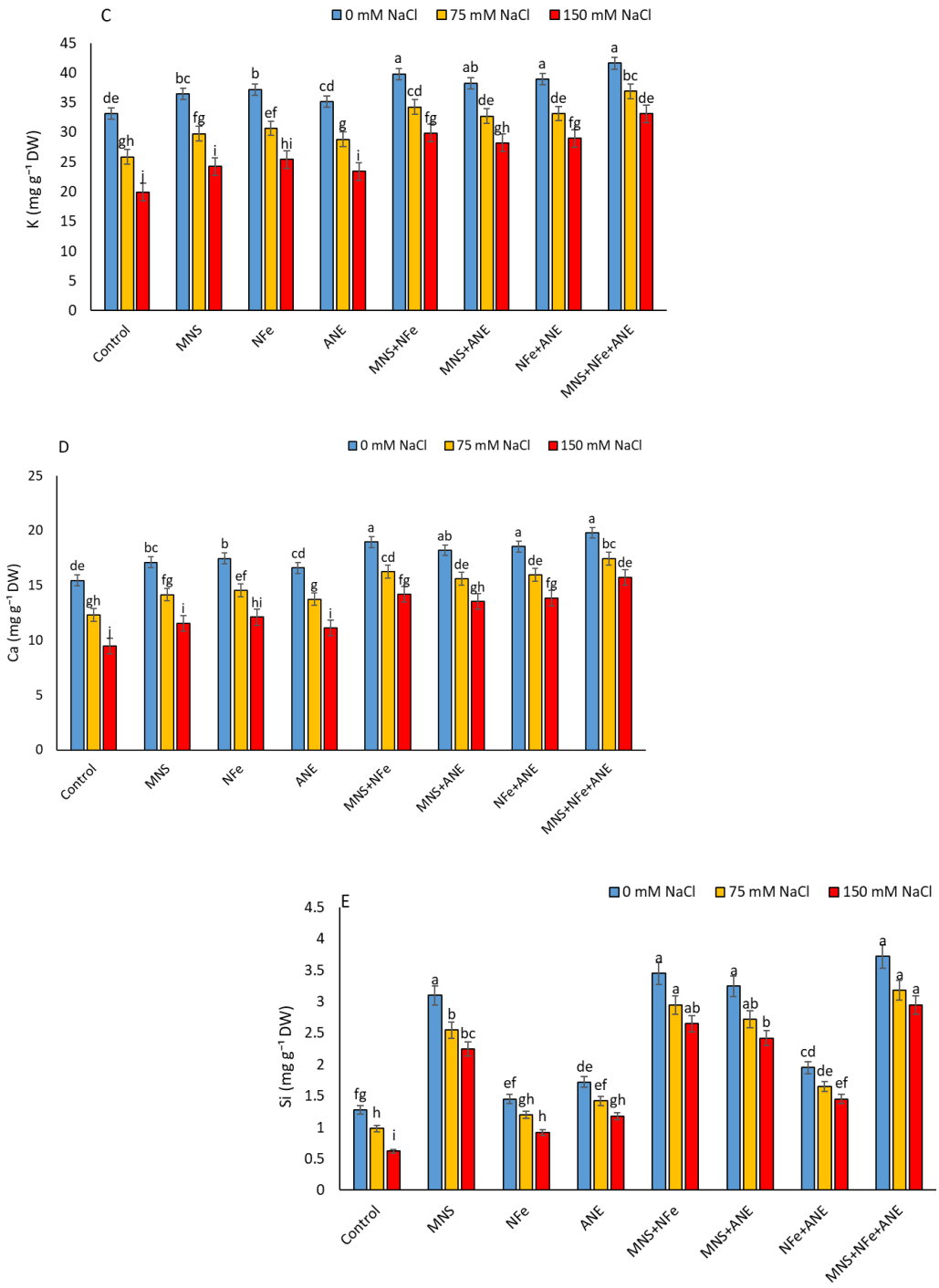


Figure 4. Effects of mesoporous nano-silica (MNS), nano-iron (NFe), and *Ascophyllum nodosum* extract (ANE), applied individually or in combination, on macronutrient and silicon contents in maize plants under different salinity levels (0, 75, and 150 mM NaCl). (A) Nitrogen (N), (B) phosphorus (P), (C) potassium (K), (D) calcium (Ca), and (E) silicon (Si) contents. Values are

presented as means ± SE. Different letters above the bars indicate significant differences among treatments according to the LSD test at $p \leq 0.05$.

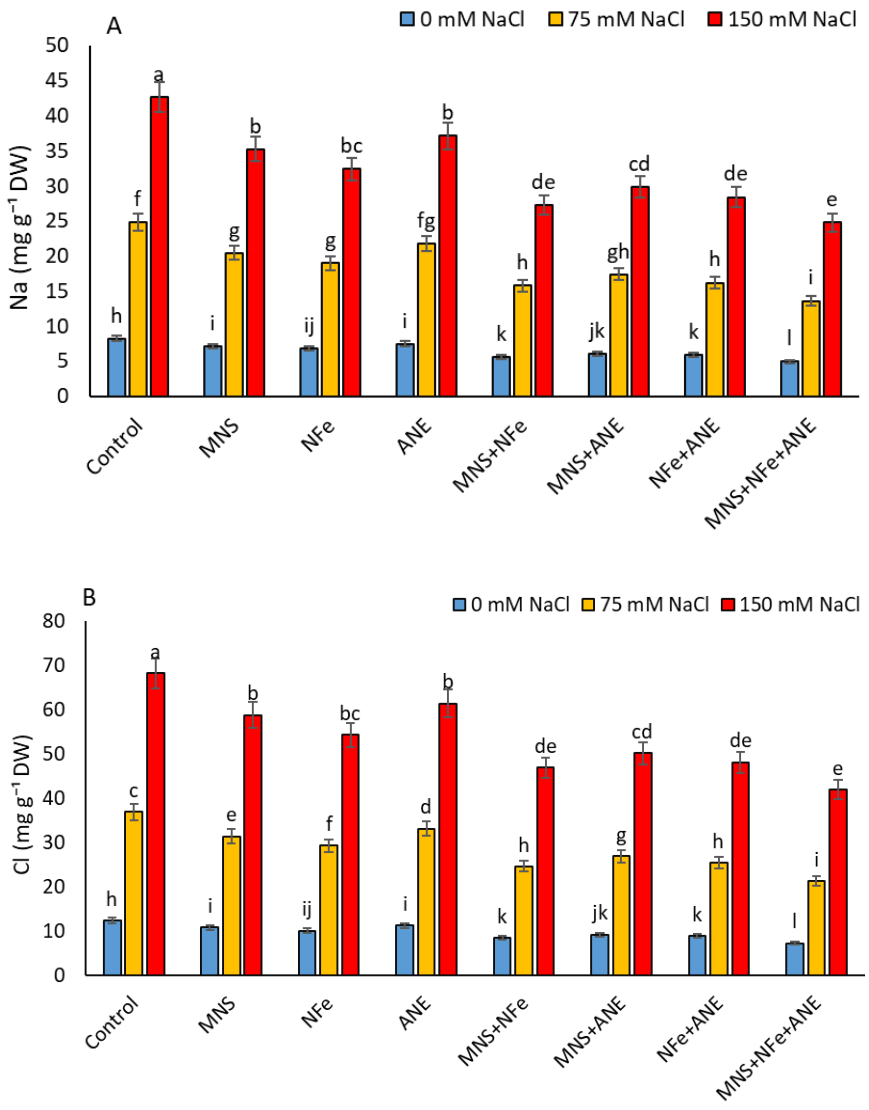
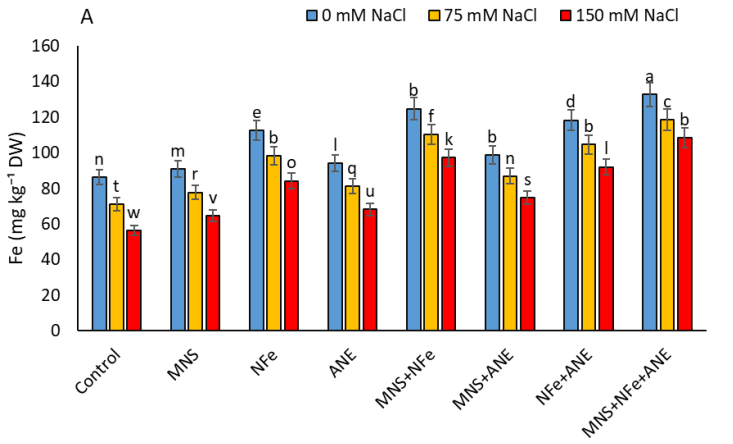
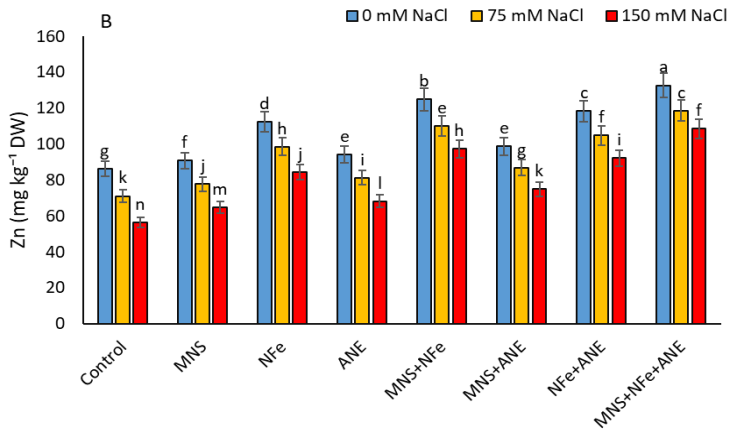


Figure 5. Effects of mesoporous nano-silica (MNS), nano-iron (NFe), and *Ascophyllum nodosum* extract (ANE), applied individually or in combination, on ionic accumulation in maize plants under different salinity levels (0, 75, and 150 mM NaCl). (A) Sodium (Na^+) and (B) chloride (Cl^-)

contents. Values are presented as means ± SE of four replicates. Different letters above the bars indicate significant differences among treatments according to the LSD test at $p \leq 0.05$.





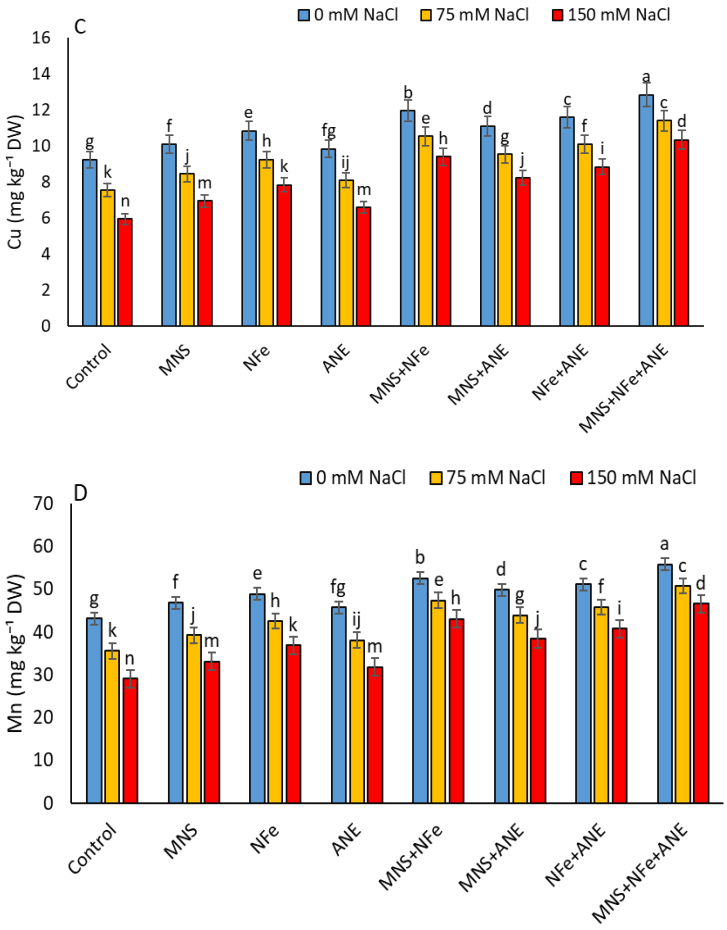


Figure 6. Effects of mesoporous nano-silica (MNS), nano-iron (NFe), and *Ascophyllum nodosum* extract (ANE), applied individually or in combination, on micronutrient accumulation in maize plants under different salinity levels (0, 75, and 150 mM NaCl). (A) Iron (Fe), (B) zinc (Zn), (C) copper (Cu), and (D) manganese (Mn) contents. Values are presented as means ± SE of four replicates. Different letters above the bars indicate significant differences among treatments according to the LSD test at $p \leq 0.05$.

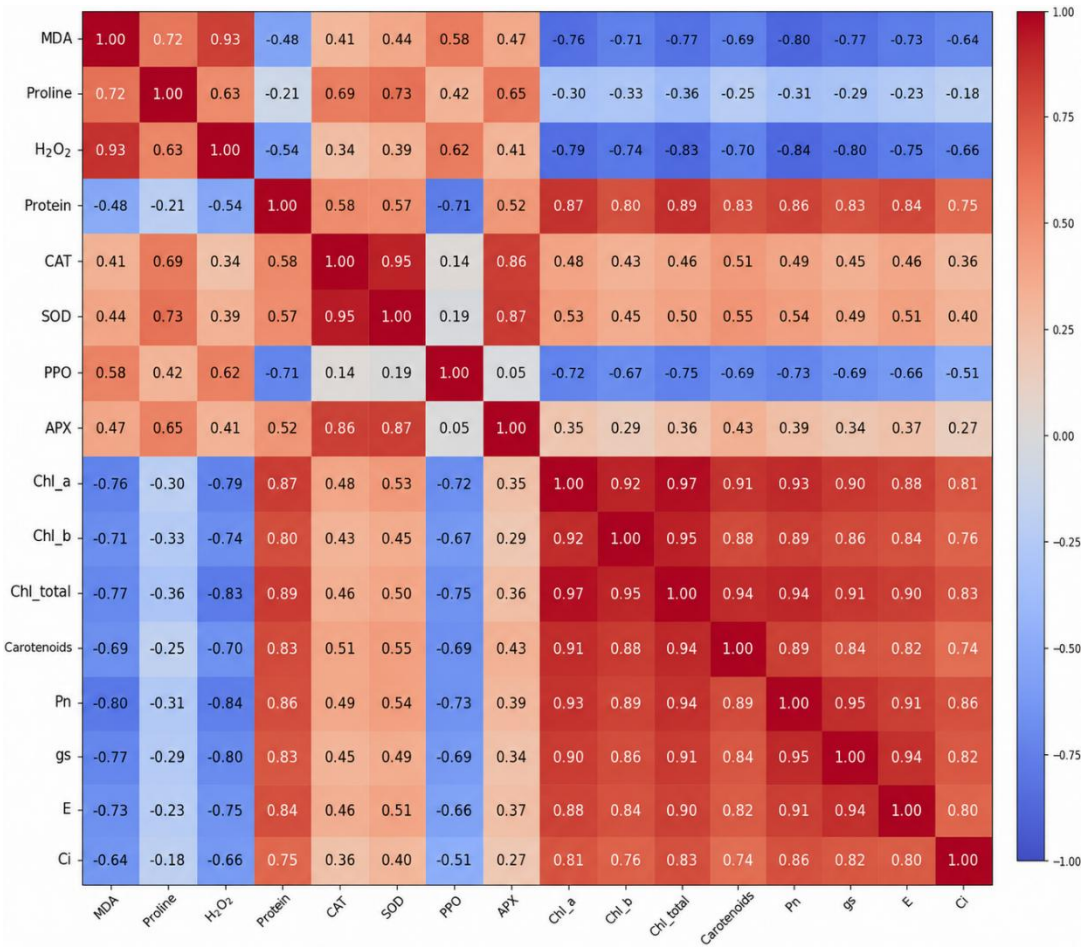


Figure 7. Pearson correlation heatmap illustrating the relationships among biochemical, antioxidant, photosynthetic pigment, and gas exchange parameters in safflower plants subjected to salinity stress and nanoparticle–biostimulant treatments. The color scale ranges from strong negative correlations (blue) to strong positive correlations (red). MDA: malondialdehyde; H_2O_2: hydrogen peroxide; CAT: catalase; SOD: superoxide dismutase; PPO: polyphenol oxidase; APX: ascorbate peroxidase; Chl a: chlorophyll a; Chl b: chlorophyll b; Chl total: total chlorophyll; Pn: net photosynthetic rate; gs: stomatal conductance; E: transpiration rate; and Ci: intercellular CO_2 concentration. Numerical values within each cell represent Pearson correlation coefficients (r).